geosciences

MDPI

Article

Outboard Onset of Ross Orogen Magmatism and Subsequent Igneous and Metamorphic Cooling Linked to Slab Rollback during Late-Stage Gondwana Assembly

Timothy Paulsen [1,*], John Encarnación [2], Anne Grunow [3], Jeffrey Benowitz [4], Paul Layer [4], Chad Deering [5] and Jakub Sliwinski [6]

1 Department of Geology, University of Wisconsin Oshkosh, Oshkosh, WI 54901, USA
2 Department of Earth and Atmospheric Sciences, Saint Louis University, St. Louis, MO 63103, USA
3 Byrd Polar Research Center, The Ohio State University, Columbus, OH 43210, USA
4 Geophysical Institute, University of Alaska Fairbanks, Fairbanks, AK 99775, USA
5 Department of Geological and Mining Engineering and Sciences, Michigan Technological University, Houghton, MI 49931, USA
6 Department of Earth Sciences, Institute of Geology, ETH Zurich, 8092 Zurich, Switzerland
* Correspondence: paulsen@uwosh.edu

Abstract: Changes in magmatism and sedimentation along the late Neoproterozoic-early Paleozoic Ross orogenic belt in Antarctica have been linked to the cessation of convergence along the Mozambique belt during the assembly of East-West Gondwana. However, these interpretations are non-unique and are based, in part, on limited thermochronological data sets spread out along large sectors of the East Antarctic margin. We report new $^{40}Ar/^{39}Ar$ hornblende, muscovite, and biotite age data for plutonic (n = 13) and metasedimentary (n = 3) samples from the Shackleton–Liv Glacier sector of the Queen Maud Mountains in Antarctica. Cumulative $^{40}Ar/^{39}Ar$ age data show polymodal age peaks (510 Ma, 491 Ma, 475 Ma) that lag peaks in U-Pb igneous crystallization ages, suggesting igneous and metamorphic cooling following magmatism within the region. The $^{40}Ar/^{39}Ar$ ages are similar to ages in other sectors of the Ross orogen, but younger than detrital mineral $^{40}Ar/^{39}Ar$ cooling ages indicative of older magmatism and cooling of unexposed inboard areas along the margin. Detrital zircon trace element abundances suggest that the widespread onset of magmatism in outboard localities of the orogen correlates with a ~560–530 Ma decrease in crustal thickness. The timing of crustal thinning recorded by zircon in magmas overlaps with other evidence for the timing of crustal extension, suggesting that the regional onset of magmatism with subsequent igneous and metamorphic cooling probably reflects slab rollback that coincided with possible global plate motion changes induced during the final assembly of Gondwana.

Keywords: $^{40}Ar/^{39}Ar$; cooling; magmatism; zircon; trace elements; slab rollback; Ross orogen; Antarctica; Gondwana

Citation: Paulsen, T.; Encarnación, J.; Grunow, A.; Benowitz, J.; Layer, P.; Deering, C.; Sliwinski, J. Outboard Onset of Ross Orogen Magmatism and Subsequent Igneous and Metamorphic Cooling Linked to Slab Rollback during Late-Stage Gondwana Assembly. *Geosciences* **2023**, *13*, 126. https://doi.org/10.3390/geosciences13040126

Academic Editors: Salvatore Critelli and Jesus Martinez-Frias

Received: 23 February 2023
Revised: 9 April 2023
Accepted: 17 April 2023
Published: 21 April 2023

1. Introduction

The continental rock record is punctuated by orogenic events associated with the closure of ocean basins during the Wilson cycle [1,2]. In many cases, these periods of orogenesis are marked within the rock record by changes in erosion and sedimentation [3], the production and preservation of igneous and metamorphic rocks [4–6], and the cooling of igneous and metamorphic terranes [7]. According to standard plate tectonic models, the closure of ocean basins associated with the collision of continents during supercontinent assembly should result in changes in plate motions along other active plate boundaries and/or the formation of new plate boundaries [8]. This may have been the case for the collision of East and West Gondwana, where the final suturing of continental fragments along the Mozambique belt (East African orogen) in the interior of Gondwana has been

argued to have led to changes in plate convergence along the paleo-Pacific margin of Gondwana (Figure 1) [2,3,9]. Evaluating potential links between these processes requires an understanding of the detailed evolution of sedimentation, magmatism, and metamorphism within Gondwana's mobile belts. However, the tectonic evolution of large sectors of Gondwana's paleo-Pacific margin remain poorly understood in Antarctica because of the incomplete exposure, remoteness, and inaccessibility of the area. $^{40}Ar/^{39}Ar$ analyses of common potassium-bearing minerals, such as hornblende, muscovite, and biotite, represent a powerful tool for constraining the thermochronological evolution of metamorphic and igneous rocks within orogenic belts for temperatures ranging from ~540° to 375 °C. Yet, there have only been a limited number of $^{40}Ar/^{39}Ar$ analyses conducted on rocks from large sectors of Gondwana's paleo-Pacific margin as is the case, for example, in the Queen Maud Mountains sector of the Ross orogenic belt in Antarctica. This contribution focuses on providing a substantial new $^{40}Ar/^{39}Ar$ data set to constrain the ages of igneous and metamorphic cooling within the Queen Maud Mountains. We also present new analyses of zircon U-Pb age and trace element data to better constrain the widespread onset of igneous and metamorphic activity and subsequent cooling in the presently exposed outboard sectors of the margin (Figure 1). Throughout this paper, we use the 2015 International Chronostratigraphic Chart time scale [10].

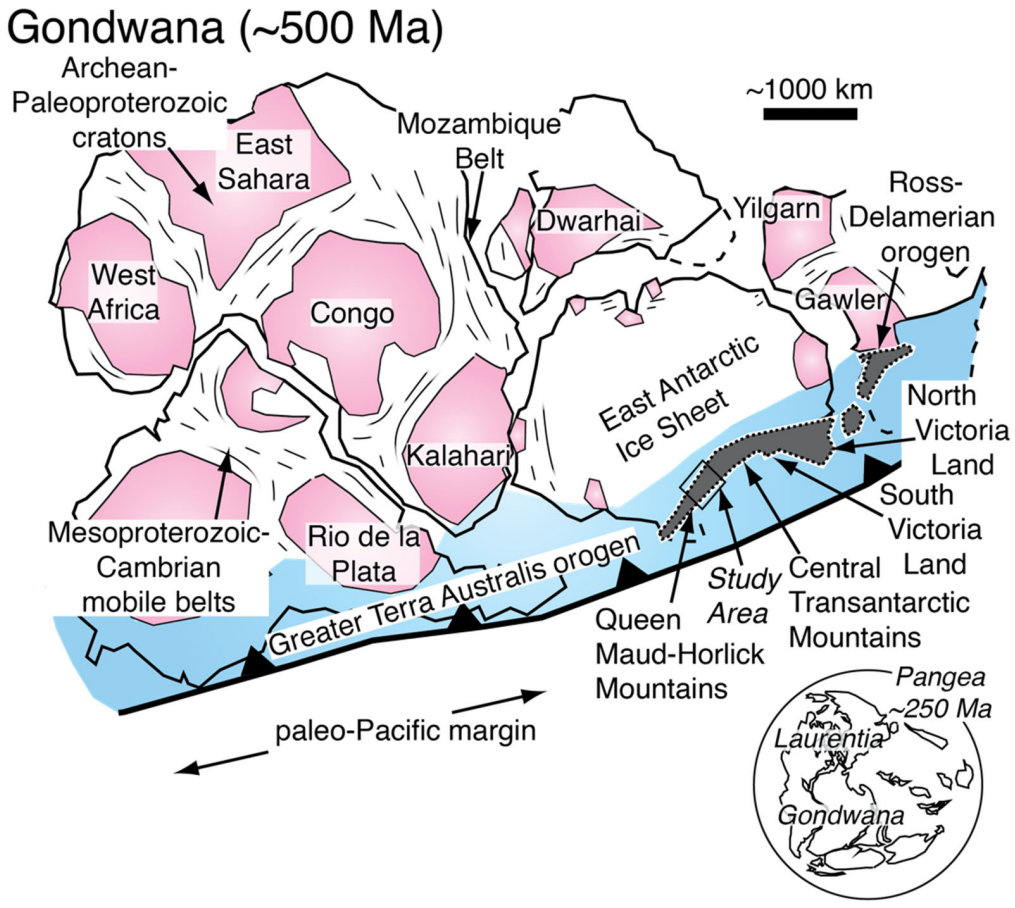

Figure 1. Gondwana reconstruction (~500 Ma) showing the Ross–Delamerian orogen within the greater latest Neoproterozoic to late Paleozoic Terra Australis orogen along the paleo-Pacific margin of Gondwana, as well as the major Precambrian cratons and mobile belts of Gondwana. Inset shows Gondwana within Pangea reconstruction (~250 Ma). Figure modified from [11,12].

2. Geology of the Queen Maud Mountains

The Queen Maud Mountains form the southern-most areas of the Transantarctic Mountains, a major mountain range located on the edge of the largely ice and snow-

covered interior of cratonic Antarctica (Figure 2) [13]. The erosional remnants of the Ross orogenic belt are found throughout the Transantarctic Mountains where they lie below the Kukri peneplain, a regionally extensive unconformity that is overlain by relatively undeformed Devonian–Jurassic sedimentary rocks of the Beacon Supergroup [14]. In the Queen Maud Mountains, sedimentary rocks involved in the Neoproterozoic to early Paleozoic Ross orogeny belong to the Ross Supergroup [15]. These rocks are typically metamorphosed in the greenschist to amphibolite facies, gently to tightly folded, and possess weak to pervasive pressure-solution cleavage and metamorphic foliation [15].

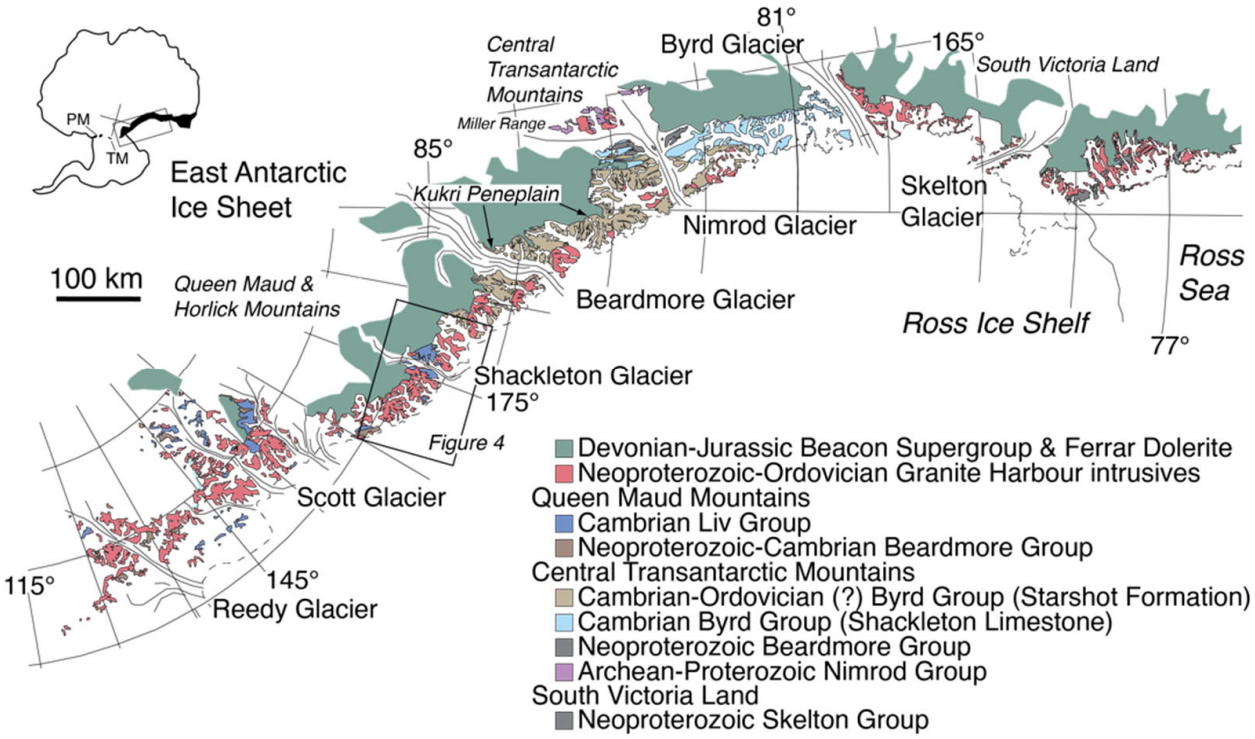

Figure 2. Simplified geologic map showing intrusive, volcanic, sedimentary, and metamorphic basement rocks of the Ross orogen and unconformably overlying Beacon Supergroup from the south Victoria Land to the south through the Queen Maud and Horlick mountains. There are abundant volcanic rocks in the early to middle Cambrian stratigraphic packages (i.e., the Liv Group) in the Queen Maud Mountains, whereas the early to middle Cambrian stratigraphic packages (i.e., the Byrd group) in the central Transantarctic Mountains are practically devoid of volcanic rocks. The boundary separating the Liv Group from the Byrd Group occurs west of Shackleton Glacier. Inset shows the location of the Transantarctic Mountains (the black area is the Ross orogen). Abbreviations: PM, Pensacola Mountains; TM, Thiel Mountains. Figure compiled and modified from others [16–20].

Early field mapping separated the Ross Supergroup into two distinct tectonostratigraphic packages known as the Beardmore and Liv groups (Figures 2 and 3) [18]. In the Queen Maud Mountains, the Beardmore Group includes siliciclastic rocks known as the La Gorce, Duncan, Goldie (remapped as Starshot Formation in part by [21,22]), and Party formations [15,16,18,23–25], the first three of which have yielded Ediacaran to Cambrian (Terreneuvian) detrital U-Pb zircon maximum depositional ages [26,27]. These ages are significantly younger than the maximum depositional ages yielded by from the Beardmore Group in the central Transantarctic Mountains [21,28] but are close to the youngest maximum depositional age yielded by a Skelton Group sample in south Victoria Land [29]. The Liv Group, in turn, includes volcanic and volcaniclastic rocks (dacites, basalts, basaltic andesites, and rhyolites) interbedded with carbonate and siliciclastic rocks [30] known as the Wyatt, Ackerman, Leverett, Taylor, Fairweather, and Greenlee formations [15,16,18,30–32]. Biostratigraphic and U-Pb zircon analyses have yielded Cambrian (Terreneuvian to Furon-

gian) ages for sedimentary and volcanic rocks of the Liv Group [27,33–36]. These ages indicate that rocks belonging to the Liv Group are at least in part temporal correlatives to the Cambrian Byrd Group (Shackleton Limestone and Douglas and Starshot formations) in the central Transantarctic Mountains (Figure 3) [21,22,37,38].

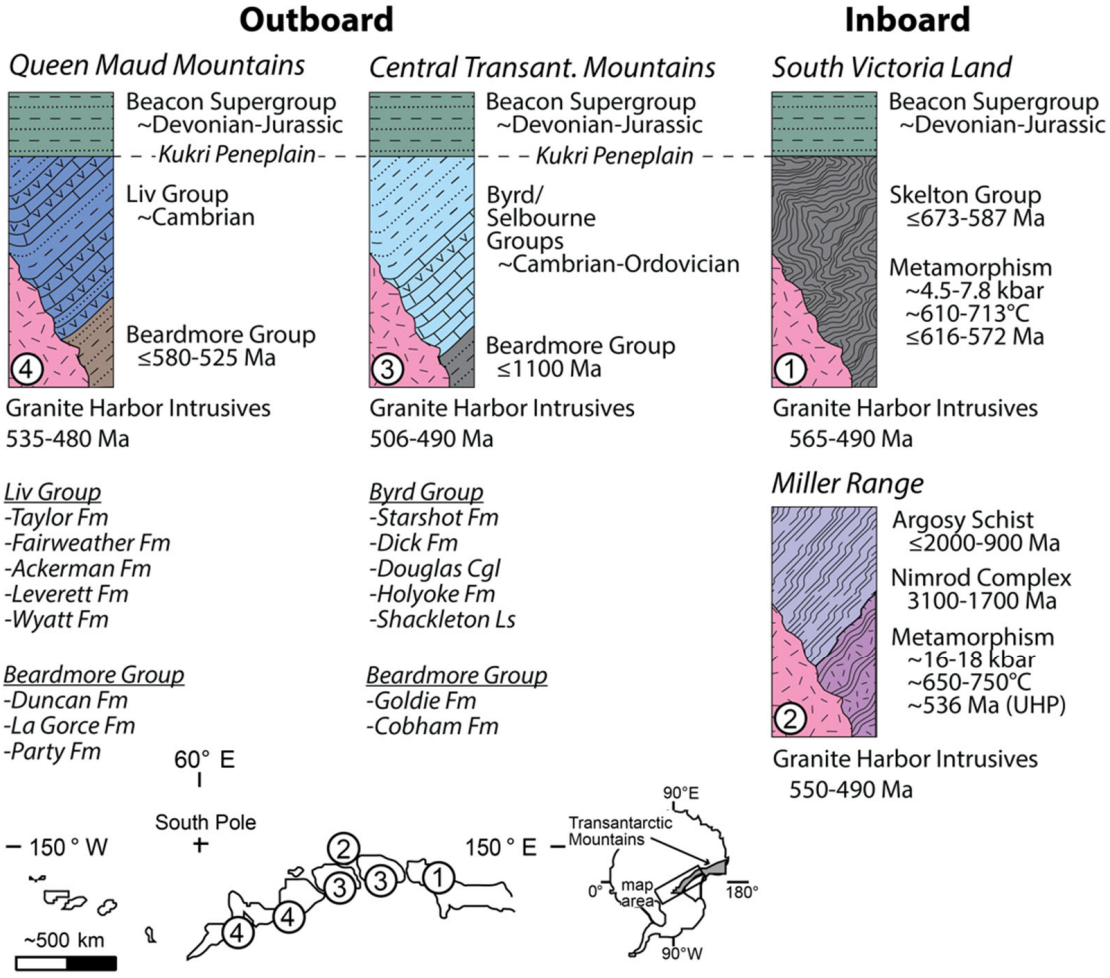

Figure 3. Schematic diagram summarizing the geology of the major rock packages found at outboard localities in the Queen Maud and central Transantarctic Mountains with respect to those found at inboard localities in the Miller Range and south Victoria Land. Ages and metamorphic conditions from sources provided in text.

Metasedimentary rocks belonging to the Beardmore and Liv groups are commonly cross-cut by intrusive rocks (Granite Harbor Intrusives) of the Queen Maud batholith (Figures 2 and 3) [15,39–41]. Igneous rocks of the batholith [15,39–41] come in undeformed and deformed suites [41] and range from granite to gabbro in composition with isotopic signatures indicative of mantle and Precambrian basement sources [40,42,43]. Zircon U-Pb geochronology indicates that intrusive activity primarily occurred within the Cambrian to Ordovician during the 535 to 480 Ma time interval [34,44–48]. Early K-Ar and Rb-Sr geochronology suggested that some intrusions and volcanic country rocks of the Queen Maud batholith crystallized and cooled as early as the Late Proterozoic [49,50], but many of these older ages suffered from large uncertainties, possible excess Ar, and open system behavior. The limited $^{40}Ar/^{39}Ar$ data that exist for the Queen Maud batholith (n = 9) and its metasedimentary country rocks (n = 2) show ca. 509–475 Ma metamorphic and igneous cooling ages [45,46,48,51–53]. There are, however, proximal low-grade metasandstones (Starshot Formation in Figure 4) that have yielded older (~570–530 Ma) detrital muscovite $^{40}Ar/^{39}Ar$ cooling ages [54]. Thus, in an attempt to further evaluate cooling

patterns ranging from ~540° to 375 °C in this outboard sector of the Ross orogenic belt, we conducted new $^{40}Ar/^{39}Ar$ (n = 20) analyses of hornblende, muscovite, and biotite from metasedimentary and intrusive igneous bedrock samples from the Shackleton to Liv Glacier area (Figure 4). The data provide substantial new information about the timing of igneous and metamorphic cooling, as well as deposition and deformation, associated with the tectonothermal evolution of the Ross orogenic belt along the paleo-Pacific margin of Gondwana.

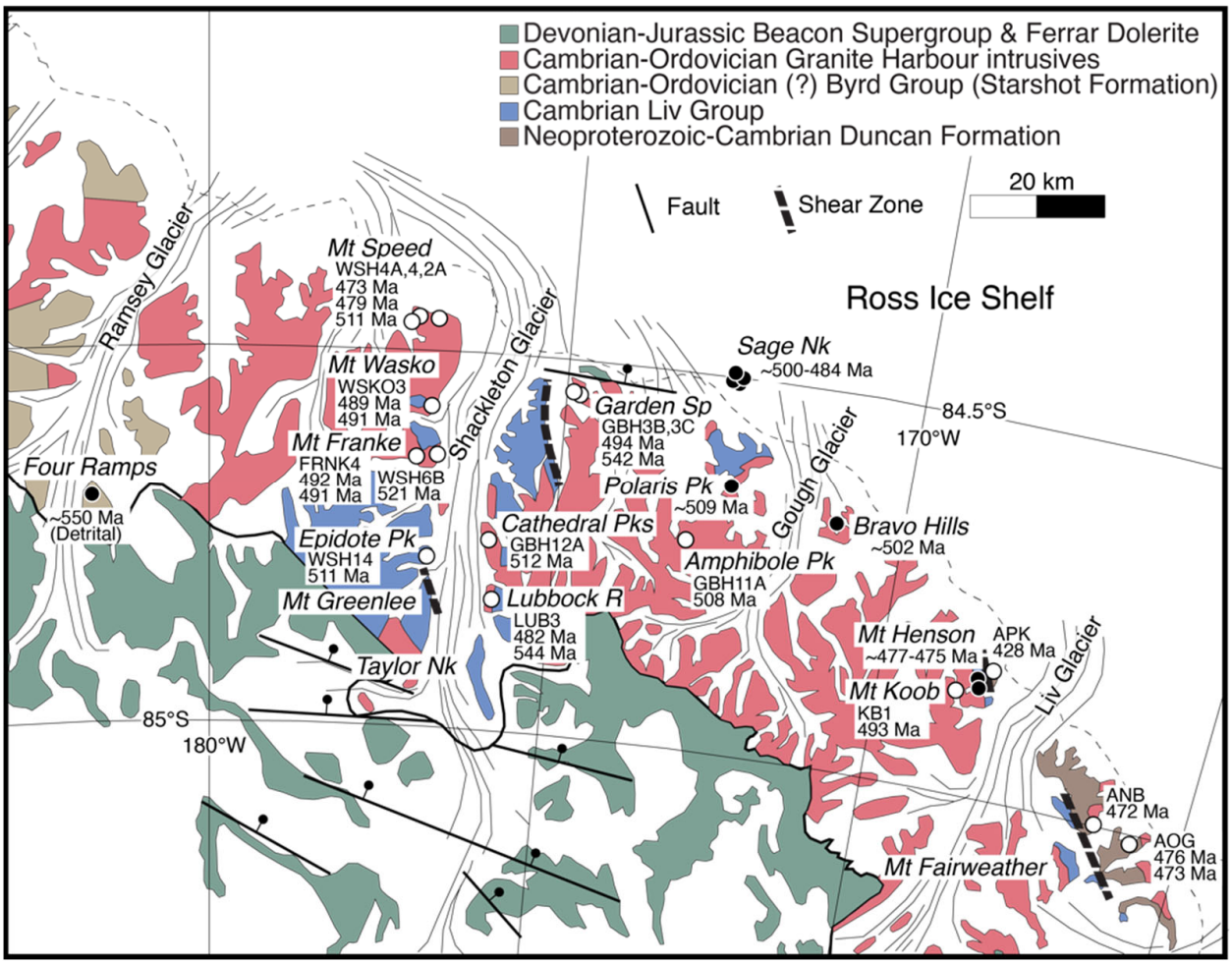

Figure 4. Simplified map showing the bedrock sample localities and geology in the Ramsey, Shackleton, and Liv Glacier areas (modified from [18]. White circles show localities of metasedimentary and intrusive rock samples analyzed herein using $^{40}Ar/^{39}Ar$ method. Black circles show locations of previous $^{40}Ar/^{39}Ar$ analyses of intrusive rocks and sedimentary rocks reported in [45,48,51,54]. The Cambria–Ordovician Starshot Formation in the Ramsey Glacier area was originally mapped as Goldie Formation but shown as Starshot Formation after [37].

3. Materials and Methods

We obtained sixteen bedrock samples from the Polar Rock Repository at The Ohio State University (see https://prr.osu.edu/, accessed on 15 February 2023) and personal collections with appropriate potassium-bearing minerals from key areas to further define igneous and metamorphic cooling patterns over the region. These samples were submitted to the Geochronology laboratory at the University of Alaska Fairbanks for $^{40}Ar/^{39}Ar$ analysis where they were crushed, sieved, washed, and hand-picked for pure hornblende, muscovite, and biotite mineral phase separates. The monitor mineral MMhb-1 [55] with an age of 523.5 Ma [56] was used to monitor neutron flux (and calculate the irradiation parameter, J). The samples and standards were wrapped in aluminum foil and loaded into

aluminum cans that were 2.5 cm diameter and 6 cm height. The samples were irradiated in position 5c of the uranium-enriched research reactor of McMaster University in Hamilton, Ontario, Canada for 20 MWh.

Upon their return from the reactor, the samples and monitors were loaded into 2 mm diameter holes in a copper tray that was then loaded in an ultra-high vacuum extraction line. The monitors were fused, and the samples were heated, using a 6-watt argon-ion laser following the technique described in [57–60]. Argon purification was achieved using a liquid nitrogen cold trap and an SAES Zr-Al getter at 400 °C. The samples were analyzed in a VG-3600 mass spectrometer at the Geophysical Institute, University of Alaska Fairbanks. The argon isotopes measured were corrected for system blank and mass discrimination, as well as calcium, potassium, and chlorine interference reactions following procedures outlined in [61]. Typical full-system 8 min laser blank values (in moles) were generally 2×10^{-16} mol ^{40}Ar, 3 × 10,218 mol ^{39}Ar, 9×10^{-18} mol ^{38}Ar, and 2×10^{-18} mol ^{36}Ar, which are 10–50 times smaller than the sample/standard volume fractions. Correction factors for nucleogenic interferences during irradiation were determined from irradiated CaF_2 and K_2SO_4 as follows: $(^{39}Ar/^{37}Ar)Ca = 7.06 \times 10^{-4}$, $(^{36}Ar/^{37}Ar)Ca = 2.79 \times 10^{-4}$ and $(^{40}Ar/^{39}Ar)K = 0.0297$. Mass discrimination was monitored by running calibrated air shots. The mass discrimination during these experiments was 1.3% per mass unit. While doing our experiments, calibration measurements were made on a monthly basis to check for changes in mass discrimination with no significant variation seen during these intervals.

A summary of all the $^{40}Ar/^{39}Ar$ results is given in Supplementary Table S1 and Figure S1, with all ages quoted to the ±1 sigma level and calculated using the constants of [62]. The resulting interpreted ages are shown in Figures 5–7 in $^{40}Ar/^{39}Ar$ age spectrum diagrams. The integrated age is the age given by the total gas measured and is equivalent to a potassium-argon (K-Ar) age. The spectrum provides a plateau age if three or more consecutive gas fractions represent at least 50% of the total gas release and are within two standard errors of each other (mean square weighted deviation less than or equal to 2.5).

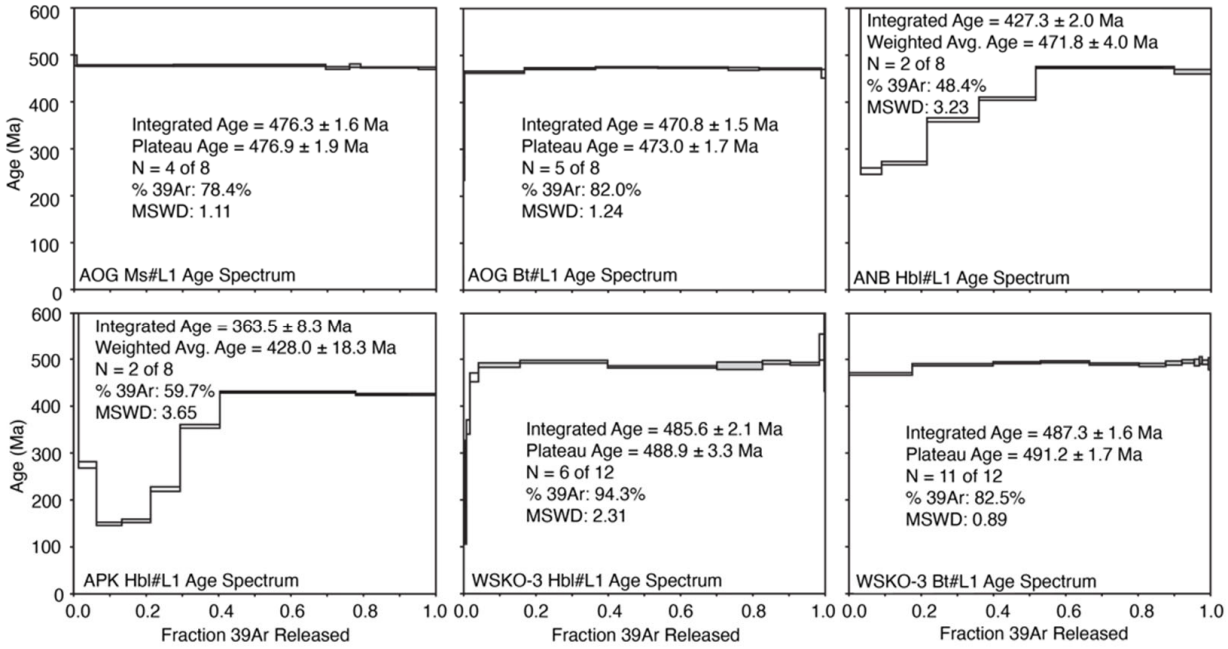

Figure 5. $^{40}Ar/^{39}Ar$ incremental release spectra for hornblende (Hbl), muscovite (Ms), and biotite (Bt) mineral separates from metasedimentary rocks samples from the Duncan Mountains and Mount Wasko. Vertical axes represent age (Ma), and horizontal axes represent cumulative percent of ^{39}Ar released. Ages in the figure are reported at the ±1-sigma level but are reported at the ±2-sigma level in the text for the sake of comparison to other geochronological constraints. Steps filled in grey were used for plateau and weighted average age determinations.

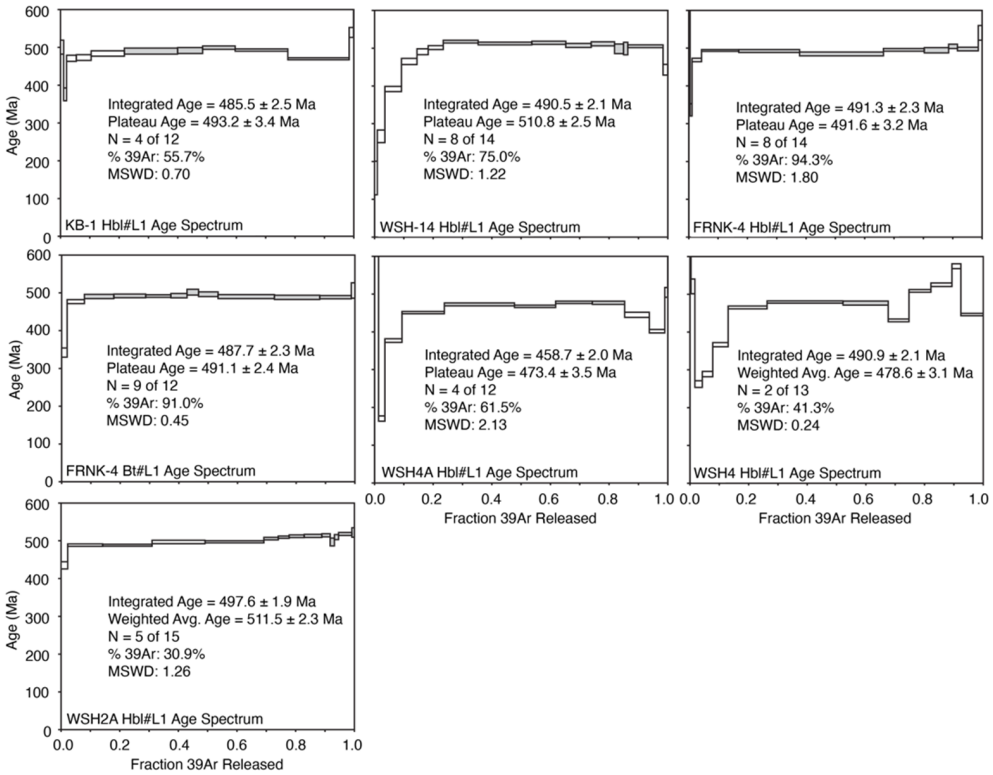

Figure 6. $^{40}Ar/^{39}Ar$ incremental release spectra for hornblende (Hbl) and biotite (Bt) mineral separates from foliated intrusive rock sample in the study area. Vertical axes represent age (Ma), and horizontal axes represent cumulative percent of ^{39}Ar released. Ages in the figure are reported at the ±1-sigma level but are reported at the ±2-sigma level in the text for the sake of comparison to other geochronological constraints. Steps filled in grey were used for plateau and weighted average age determinations.

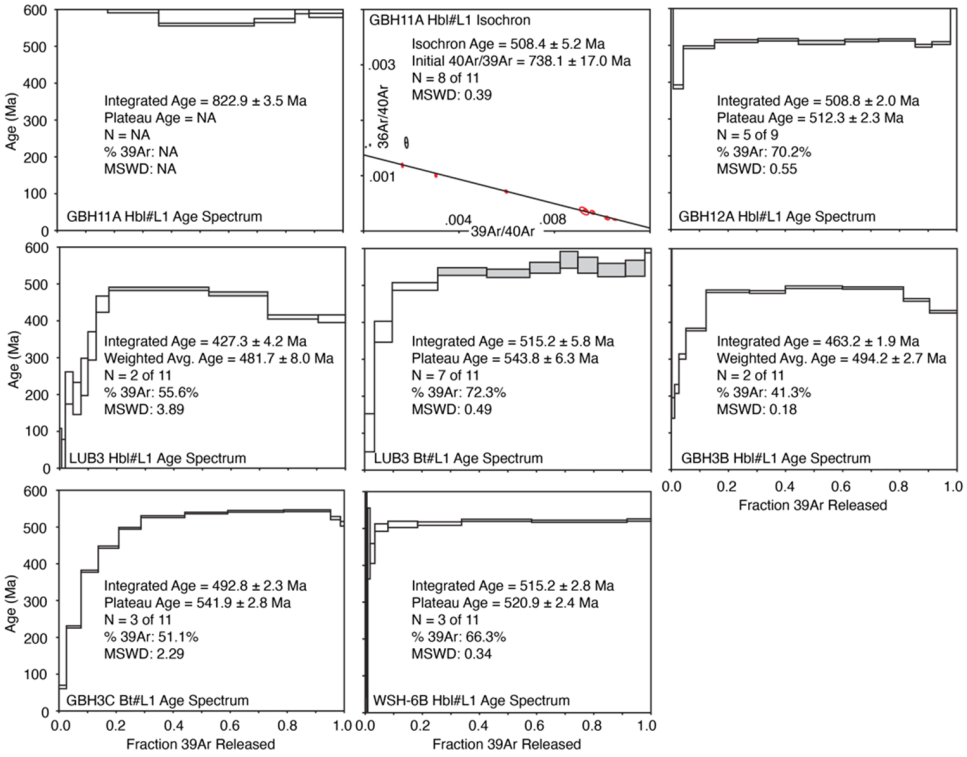

Figure 7. $^{40}Ar/^{39}Ar$ incremental release spectra for hornblende (Hbl) and biotite (Bt) mineral separates from unfoliated intrusive rock sample in the study area. Vertical axes represent age (Ma) and

horizontal axes represent cumulative percent of ^{39}Ar released. Ages in the figure are reported at the ±1-sigma level but are reported at the ±2-sigma level in the text for the sake of comparison to other geochronological constraints. Steps filled in grey were used for plateau and weighted average age determinations. Uncertainty ellipses filled in red were the steps used for isochron age determination.

The names of samples discussed in the next section that are in parenthesis (with a PRR prefix) are the assigned sample IGSN's (International Generic Sample Number) from the Polar Rock Repository.

4. Results

4.1. Metasedimentary Rocks

We analyzed hornblende (n = 2), muscovite (n = 1), and biotite (n = 1) separated from three metasedimentary schist samples from the Duncan Formation that include two samples from Mount Fairweather (AOG, ANB) and one sample from Mount Henson (APK) in the Liv Glacier area (Figure 4 and Figure S2). We also analyzed hornblende (n = 1) and biotite (n = 1) from one sample from the lower Shackleton Glacier area. Four analyses (1 hornblende, 1 muscovite and 2 biotite) yielded spectra that met the criteria for a plateau age, whereas two analyses (hornblende) did not, and a weighted mean age of high-temperature steps is reported instead (Figure 5).

Sample AOG is a muscovite biotite schist collected by Edmund Stump from the Duncan Formation ~10 km to the northeast of Mount Fairweather on ridge 13 (Figure 4) [63]. Muscovite from sample AOG produced a ^{40}Ar/^{39}Ar plateau age of 476.9 ± 3.8 Ma (2 sigma; 4 fractions, 78% ^{39}Ar release, MSWD = 1.1) that is within uncertainty of the 476.3 ± 3.8 Ma (2 sigma) integrated age (Figure 5). Biotite from sample AOG produced a ^{40}Ar/^{39}Ar plateau age of 473.0 ± 3.4 Ma (2 sigma; 5 fractions, 82% ^{39}Ar release, MSWD = 1.24) that is within uncertainty of the 470.8 ± 3.0 Ma (2 sigma) integrated age (Figure 5). The initial incremental heating steps of the AOG muscovite and biotite analyses had high atmospheric content indicative of alteration and are not used in the age determination. The 476.9 ± 3.8 Ma (muscovite) and 473.0 ± 3.4 Ma (biotite) plateau ages are considered to be the ^{40}Ar/^{39}Ar cooling ages of these mineral phases. These cooling ages are consistent with detrital zircon U-Pb maximum depositional age peaks (549 Ma and 539 Ma) yielded by separate samples of the Duncan Formation (Figure 8A) [27,54].

Sample ANB is a hornblende schist collected by Edmund Stump from the Duncan Formation ~8 km to the north of Mount Fairweather on ridge 10 (Figure 4) [63]. Hornblende from sample ANB produced an incremental step-heat-release pattern with a stepping-up age pattern where the higher-temperature steps had older ages than the lower-temperature steps (Figure 5). This pattern is indicative of gas loss associated with alteration or reheating. The 427.3 ± 4.0 Ma (2 sigma) integrated age and the 471.8 ± 8.0 Ma weighted mean age (2 sigma; 2 fractions, 48% ^{39}Ar release, MSWD = 3.23) are not within uncertainty. The 471.8 ± 8.0 Ma weighted mean age is the preferred age because of the documented loss and is interpreted as the minimum ^{40}Ar/^{39}Ar cooling age of this mineral phase.

Sample APK is a hornblende schist collected by Edmund Stump from the Duncan Formation at Mount Henson (Figure 4) [24,25,63]. Hornblende from sample APK produced an incremental step-heat-release pattern with a stepping-up age pattern where the higher-temperature steps had older ages than the lower-temperature steps (Figure 5). This pattern is indicative of gas loss associated with alteration or reheating. The 363.5 ± 16.6 Ma (2 sigma) integrated age and the 428.0 ± 36.6 Ma weighted mean age (2 sigma; 2 fractions, 60% ^{39}Ar release, MSWD = 3.65) were not within uncertainty. The 428.0 ± 18.3 Ma weighted mean age is the preferred age because of the documented loss. Of note, the Ca/K ratio was greater than 15 for the steps chosen, which is high for hornblende but low for actinolite. We therefore interpret the age of 428.0 ± 36.6 Ma as reflecting the ^{40}Ar/^{39}Ar alteration age of this mineral phase.

Sample WSKO-3 (PRR14032) is an amphibolite gneiss with a possible sedimentary protolith collected by John Burgener from a ridge 5 km west–southwest of Mount Wasko (Figure 4) [64]. Hornblende and biotite were dated from this sample, and both produced very flat age spectra and plateau ages of 488.9 ± 6.6 (2 sigma; 6 fractions, 94% ^{39}Ar release, MSWD = 2.31) and 491.2 ± 3.4 Ma (2 sigma; 11 fractions, 86% ^{39}Ar release, MSWD = 0.89), respectively (Figure 5). The biotite is slightly older than the hornblende mineral phase from this sample due to a slight "hump-shaped" character reflective of a minor amount of ^{39}Ar recoil.

4.2. Foliated/Pretectonic Intrusive Rocks

Early field investigations in the Shackleton Glacier area classified intrusions with secondary, solid-state foliations as being pretectonic to syntectonic in age, whereas intrusive bodies lacking such fabrics have been considered post-tectonic in age [41]. In many cases, pretectonic and syntectonic intrusive rocks display relict crystalline igneous textures (such as relict blocky feldspar phenocrysts) within outcrops, indicating an igneous rather than sedimentary parent rock. We analyzed hornblende (n = 6), and biotite (n = 2) separated from six foliated and/or pretectonic intrusive rock samples that include one sample from the Liv Glacier area (KB1), one sample from the upper Shackleton Glacier (WSH14), and four samples (FRNK-4, WSH2A, WSH4A, WSH4) from the lower reaches of Shackleton Glacier (Figure 4 and Figure S2). Five analyses (four hornblende and one biotite) yielded spectra that met the criteria for a plateau age, two analyses (hornblende) yielded weighted mean ages, and one analysis (biotite) yielded uninterpretable results (Figure 6).

Sample KB1 (PRR13931) is a granitic gneiss collected by John Burgener from Mount Koob in the Mayer Crags region located to the western flank of Liv Glacier (Figure 4) [64]. Hornblende from sample KB1 has a ^{40}Ar/^{39}Ar plateau age of 493.2 ± 6.8 Ma (2 sigma; 4 fractions, 56% ^{39}Ar release, MSWD = 0.7) that is considered to be the ^{40}Ar/^{39}Ar cooling age of this mineral phase (Figure 6). This age is consistent with a weighted mean ^{206}Pb-^{238}U crystallization age of 515 ± 8 Ma for this sample (Figure 8A) [48]. Biotite from the same sample shows a complex age spectrum with significant argon loss and a "hump shape" indicative of ^{39}Ar recoil. This age spectrum, and an anomalously high Ca/K ratio of >1, indicates that the biotite was probably altered and does not preserve interpretable age information and is not shown on Figure 6.

Sample WSH14 (PRR5332) is a sample of a crudely foliated to unfoliated biotite granite layer collected by John Encarnación at the base of Epidote Peak along the upper reach of Shackleton Glacier where it is generally concordant with a pink sheared out fine to medium-grained felsite containing possible porphyroclasts of the granite (Figure 4). Hornblende from sample WSH14 shows a Ca/K ratio of ~7, with some evidence of argon loss at low-laser-power steps but produced a well-defined ^{40}Ar/^{39}Ar plateau age of 510.8 ± 5.0 Ma (2 sigma; 8 of 14 fractions, 75% ^{39}Ar release, MSWD = 1.22) considered to be the ^{40}Ar/^{39}Ar cooling age of this mineral phase (Figure 6). This age is broadly consistent, given the uncertainties in ages, with a weighted mean ^{206}Pb-^{238}U crystallization age of 495 ± 9 Ma (2 sigma) for an overlying felsite in which it is in contact (Figure 8B) [48].

Sample FRNK-4 (PRR13927) is a porphyritic tonalite gneiss collected by John Burgener from the northeast corner of Mount Franke on the western flank of Shackleton Glacier (Figure 4) [64]. Hornblende from sample FRNK-4 produced a well-defined ^{40}Ar/^{39}Ar plateau age of 491.6 ± 6.4 Ma (2 sigma; 7 of 11 fractions, 94% ^{39}Ar release, MSWD = 1.8) that is within uncertainty of the 491.3 ± 4.6 Ma (2 sigma) integrated age (Figure 6). Biotite from sample FRNK-4 also produced a well-defined ^{40}Ar/^{39}Ar plateau age of 491.1 ± 4.8 Ma (2 sigma; 9 of 12 fractions, 91% ^{39}Ar release, MSWD = 0.45) that is within uncertainty of the 487.6 ± 4.6 Ma (2 sigma) integrated age (Figure 6). These ages are consistent with a weighted mean ^{206}Pb-^{238}U crystallization age of 507 ± 7 Ma (2 sigma) for the sample (Figure 8C) [48].

Sample WSH4A (PRR5326) is a tonalitic amphibolite interlayered with marble collected by John Encarnación from Oppegaard Spur at Mount Speed (Figure 4). Hornblende

from sample WSH4A produced a $^{40}Ar/^{39}Ar$ plateau age of 473.4 ± 7 Ma (2 sigma; 4 of 12 fractions, 62% ^{39}Ar release, MSWD = 2.13) (Figure 6). However, the spectrum shows evidence of argon loss, and it is possible that the true $^{40}Ar/^{39}Ar$ cooling age of this mineral phase is older. For example, a model spectrum with a 490 Ma cooling age and 10% Ar loss at 100 Ma fits the data reasonably well.

Sample WSH4 (PRR5966) is a tonalite boudin encapsulated in white marble collected by John Encarnación from a northwest-trending spur north of Oppegaard Spur at Mount Speed (Figure 4). Hornblende shows evidence of alteration as seen in variable Ca/K, Cl/K and age spectra (Figure 6). The 490.9 ± 4.2 Ma (2 sigma) integrated age and the 478.6 ± 6.2 Ma weighted mean age (2 sigma; 2 fractions, 41% ^{39}Ar release, MSWD = 0.24) are not within uncertainty. As with sample 5326, it is possible that the cooling age of this sample is older than the 'plateau-like' fractions at ~480 Ma; again, a model with a cooling age of ~490 Ma and a Cretaceous loss event fits the data fairly well. This age is consistent with a weighted mean ^{206}Pb-^{238}U crystallization age of 499 ± 6 Ma (2 sigma) for the sample (Figure 8C) [48].

Sample WSH2A (PRR16884) is a strongly foliated granite collected by Anne Grunow from a northwest-trending ridge located to the northwest of a peak (900 feet above mean sea level) that lies to the north of Mount Speed (Figure 4). Hornblende from this sample produced a classical stair-step-up age spectrum (Figure 6), which we interpret to reflect minor loss alteration. Incremental heating step ages broadly correlate with Ca/K ratios and this pattern also indicates possible alteration and/or the presence of chemical heterogeneity. Given the gas-release steps up to a multi-step weighted mean age of 511.5 ± 4.6 Ma, we infer this age is representative of the $^{40}Ar/^{39}Ar$ cooling age of this mineral phase.

4.3. Unfoliated Intrusive Rocks

We analyzed hornblende (n = 6), and biotite (n = 2) separated from six unfoliated intrusive rock samples that include one sample from the Gabbro Hills (GBH11A), two samples from the upper reaches of Shackleton Glacier (GBH12A, LUB3), and three samples from the lower reaches of Shackleton Glacier (GBH3B, GBH3C, WSH6B) (Figure 4 and Figure S2). One analysis (hornblende) yielded an isochron age, four analyses (two hornblende and two biotite) yielded spectrum that met the criteria for a plateau age, two analyses (hornblende) yielded weighted mean ages, and one analysis (hornblende) yielded uninterpretable results (Figure 7).

Sample GBH11A (PRR26640) is a gabbro collected by Anne Grunow ~12 km to the southwest of Polaris Peak near Amphibole Peak (Figure 4). Hornblende from GBH11A has a significant amount of excess argon. The youngest fractions have apparent ages of 560 Ma. However, this sample does have a very well-defined isochron with an $^{40}Ar/^{39}Ar$ age of 508.4 ± 10.4 Ma (2 sigma; 8 of 11 fractions, MSWD = 0.39), which is considered to be the cooling age of this mineral (Figure 7).

Sample GBH12A (PRR5293) is a coarse equigranular biotite granite collected by John Encarnación along the base of Cathedral Peaks along the Shackleton Glacier (Figure 4). Hornblende from sample GBH12A produced a well-defined $^{40}Ar/^{39}Ar$ plateau age of 512.2 ± 4.6 Ma (2 sigma; 5 of 9 fractions, 70% ^{39}Ar release, MSWD = 0.55) for fractions with varying Ca/K and Cl/K that is considered to be the cooling age of this mineral (Figure 7).

Sample LUB3 (PRR-5951) is an unfoliated K-feldspar porphyritic medium to coarse-grained biotite granite collected by John Encarnación from the east end of Lubbock Ridge along the eastern flank of Shackleton Glacier (Figure 4). Hornblende from sample LUB3 has a hump-shaped age spectrum, which is evidence of disturbed argon isotopic systematics (Figure 7). In addition, the first ~10% of the release had very low Ca/K for hornblende and a low percentage of radiogenic argon. The two oldest steps yield a weighted mean age of 481.7 ± 16 Ma (2 sigma; 2 of 11 fractions, 56% ^{39}Ar release, MSWD = 3.89) considered to be the minimum $^{40}Ar/^{39}Ar$ cooling age for this mineral phase. This age is consistent with a weighted mean ^{206}Pb-^{238}U crystallization age of 503 ± 7 Ma (2 sigma) for the sample (Figure 8B) [48]. Biotite from sample LUB3 shows evidence of argon loss (Figure 7).

The biotite plateau age, 543.8 ± 12.6 Ma (2 sigma; 7 of 11 fractions, 72% ^{39}Ar release, MSWD = 0.49), is not reasonable given the 503 Ma ^{206}Pb-^{238}U zircon crystallization age and the 482 Ma minimum hornblende cooling age for this sample. It is also inconsistent with the 516 Ma ^{206}Pb-^{238}U crystallization age [34] and the 515 Ma ^{206}Pb-^{238}U detrital zircon maximum deposition age yielded by Taylor Formation country rocks that the granite cross cuts at this locality [27,54]. The lack of a well-constrained isochron makes it difficult to assess the contribution of excess argon. Baldwin et al. [65] reported that similar age biotite from this region of Antarctica also show anomalous excess argon, and we also conclude that the biotite sample likely incorporated excess argon.

Sample GBH3B (PRR-5932) is a sphene-bearing hornblende diorite collected by John Encarnación from the northwest-trending ridge extending from the peak (700 feet above mean sea level) located along Garden Spur (Figure 4). Hornblende from this sample produced young ages and low Ca/K ratios (alteration) during low-laser-power incremental heating steps (Figure 7). The 494.2 ± 5.4 Ma weighted mean age (2 sigma; 2 of 11 fractions, 41% ^{39}Ar release, MSWD = 0.18) may reflect this alteration and is considered to be a minimum ^{40}Ar/^{39}Ar cooling age for the hornblende mineral phase.

Sample GBH3C (PRR-5933) is an undeformed pink porphyritic granite collected by John Encarnación from the northwest tip of the northeast side of Garden Spur (Figure 4). Hornblende from sample GBH3C shows young ages and low Ca/K ratios during low-laser-power incremental heating steps, indicative of alteration. Biotite from sample GBH3C shows evidence of significant argon loss and a slight "hump shape" with younger ages at low and high ^{39}Ar release (Figure 7). The plateau age, 541.9 ± 5.6 Ma (2 sigma; 3 of 11 fractions, 51% ^{39}Ar release, MSWD = 2.29), should not be considered geologically significant given that it is older than ^{206}Pb-^{238}U zircon crystallization ages for magmatic rocks from the Queen Maud–Horlick Mountains (Figure 8D) and known issues with excess argon in neighboring samples [65]. Biotite is a known hydrous mineral that can be unstable during in vacuo laser heating [66]; thus in some cases, it may not produce geologically meaningful gas-release patterns that reflect crystal spatial Ar isotopic gradients [67]. Hence, we prefer the integrated age of 492.8 ± 4.6 Ma (2 sigma) as most representative of the ^{40}Ar/^{39}Ar cooling age for the biotite mineral phase.

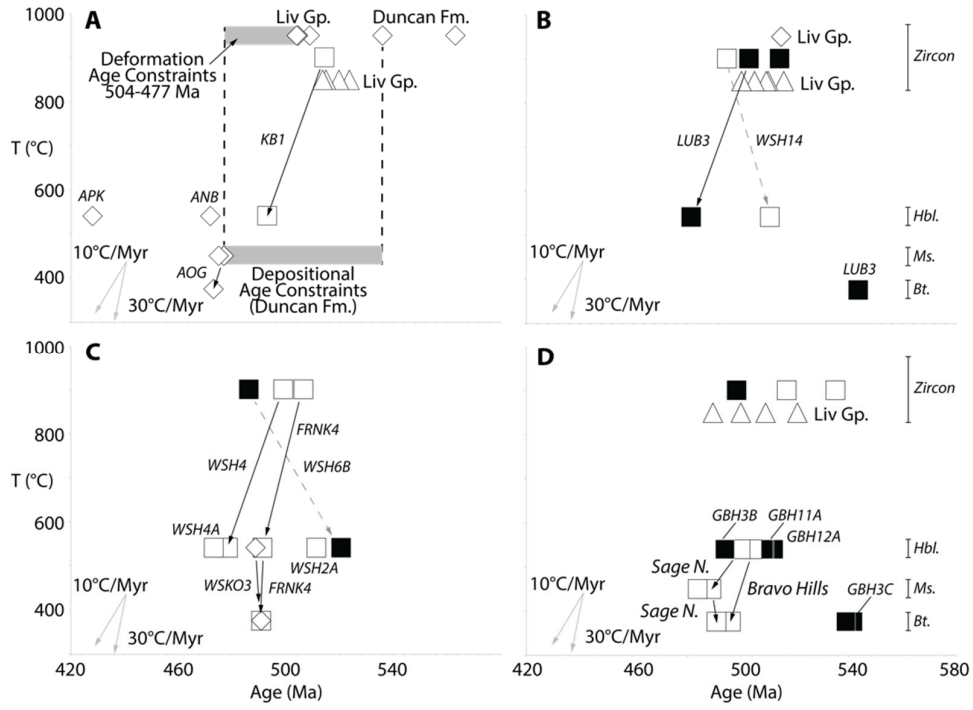

Figure 8. ^{40}Ar/^{39}Ar thermochronological data illustrating the cooling histories(of metasedimentary (diamond) and foliated/pretectonic (open) and unfoliated filled) intrusive rocks (squares) with

respect to U-Pb detrital zircon maximum depositional ages and U-Pb zircon crystallization ages for intrusive (squares) and volcanic (triangles) rocks in (**A**) Duncan Mountains, (**B**) upper Shackleton Glacier, (**C**) lower Shackleton Glacier areas, and (**D**) Gabbro Hills. Vertical axes represent temperature (T) and horizontal axes are age (Ma). Zircon U-Pb age data are plotted along, above, and below the 900 °C U-Pb closure temperature for clarity. $^{40}Ar/^{39}Ar$ nominal closure temperatures are taken to be 540 °C (hornblende, Hbl.; [68]), 450 °C (muscovite, Ms.; [69]), and 375 °C (biotite, Bt.; [70]). Arrows connect symbols for ages from different minerals from the same samples.

Sample WSH-6B (PRR-16883) is an unfoliated porphyritic granodiorite collected by Anne Grunow from the base of the south side of Mount Franke on the western flank of Shackleton Glacier (Figure 4). Hornblende from sample WSH-6B has a well-defined plateau age of 520.9 ± 4.8 Ma (2 sigma; 3 of 11 fractions, 66% ^{39}Ar release, MSWD = 0.34) for consistent Ca/K ratio fractions with values of ~1 (Figure 7). This is the oldest cooling age yet documented from the Shackleton Glacier area, but it is older than and therefore inconsistent with the 486 ± 12 Ma (2 sigma) ^{206}Pb-^{238}U zircon crystallization age yielded by a porphyritic granodiorite sample from the same locality [48]. Given the geochronologic inconsistencies reviewed above, this age should be viewed with caution unless it is verified by future work.

5. Discussion

McGregor [41] and Stump [24] recognized two phases of metamorphism within the Shackleton–Liv Glacier area. The oldest phase was associated with dynamic recrystallization attributed to deformation during the Ross orogeny. This was followed by a younger phase characterized by static recrystallization during the emplacement of younger intrusive bodies. Apatite fission track and apatite U-Th/He analyses suggest intrusive rocks in the study area passed through the 120 °C to 70 °C closure temperatures in the Eocene to Oligocene [71,72]. Our data record the last passage of igneous and metamorphic rocks through $^{40}Ar/^{39}Ar$ closure temperatures ranging from ~540 °C (hornblende) to 375 °C (biotite) in the Cambrian to Ordovician (Figure 8). Figure 9 shows a kernel-density-estimation diagram for all $^{40}Ar/^{39}Ar$ cooling ages (n = 28) obtained for intrusive rocks, as well as metasedimentary rocks, reported for the study area [35,45]. Density analysis shows the polymodal age distributions with primary 510 Ma, 491 Ma, and 475 Ma age peaks. The ~540 Ma $^{40}Ar/^{39}Ar$ age peak shown in Figure 9 reflects three older biotite $^{40}Ar/^{39}Ar$ ages, but these are likely a result from excess argon or problems associated with mineral stability during in vacuo laser heating [66]. The overall data therefore suggest that significant igneous and metamorphic cooling commenced as early as ~510 Ma in the Shackleton–Liv Glacier area.

The onset of magmatism associated with Ross orogenesis in the Queen Maud Mountains is recorded by the emplacement of ~535 Ma intrusive rocks and the ~526 Ma eruption of volcanic rocks belonging to the Wyatt Formation of the Liv Group [44,45]. Kernel density analysis for all U-Pb zircon ages (n = 27) obtained for intrusive rocks (foliated and unfoliated), as well as extrusive (volcanic) samples (Liv Group) reported for the study area, suggests that a significant magmatic flare up occurred at ~516 Ma, followed by pulses at 506–502 Ma and 488 Ma (Figure 9) [48]. These age peaks are broadly similar to detrital zircon U-Pb age peaks shown by sandstones collected from the area. Liv Group (Fairweather and Taylor formations) sandstones in particular show significant populations of ~530–490 Ma (Cambrian, ~Terreneuvian–Furongian) detrital zircons (Figure 10). These detrital zircon U-Pb age populations are close to Liv Group depositional ages yielded by biostratigraphic data of sedimentary rocks (Cambrian, Series 2 to Series 3, 521–501 Ma) [31,33,74], as well as U-Pb zircon crystallization ages (526–489 Ma) of volcanic rocks [33–35]. Siliciclastic sediments deposited in convergent margin settings are typified by high proportions of detrital zircons with U-Pb ages that approach or even overlap their depositional ages [75]. This is due to the presence of ample zircon source rocks being produced along subduction zones [76]. Conversely, siliciclastic sediments deposited in collisional, extensional, or craton

interior settings are typified by higher proportions of detrital zircons with older U-Pb ages that reflect basement source rocks [75]. Thus, the abundance of young detrital zircons in Liv Group samples implies that deposition occurred close to an active plate margin in a suprasubduction zone setting [71], a conclusion that is consistent with the widespread emplacement of calk-alkaline granitoids (i.e., the Granite Harbor intrusive suite) during the Cambrian, suggesting that the Ross orogeny was related to subduction [15,40,42,44,77,78]. The ~510 Ma $^{40}Ar/^{39}Ar$ age peak post-dates the 516 Ma igneous age peak shown in Figure 9, suggesting that significant igneous and metamorphic cooling commenced following the onset of magmatism in the area.

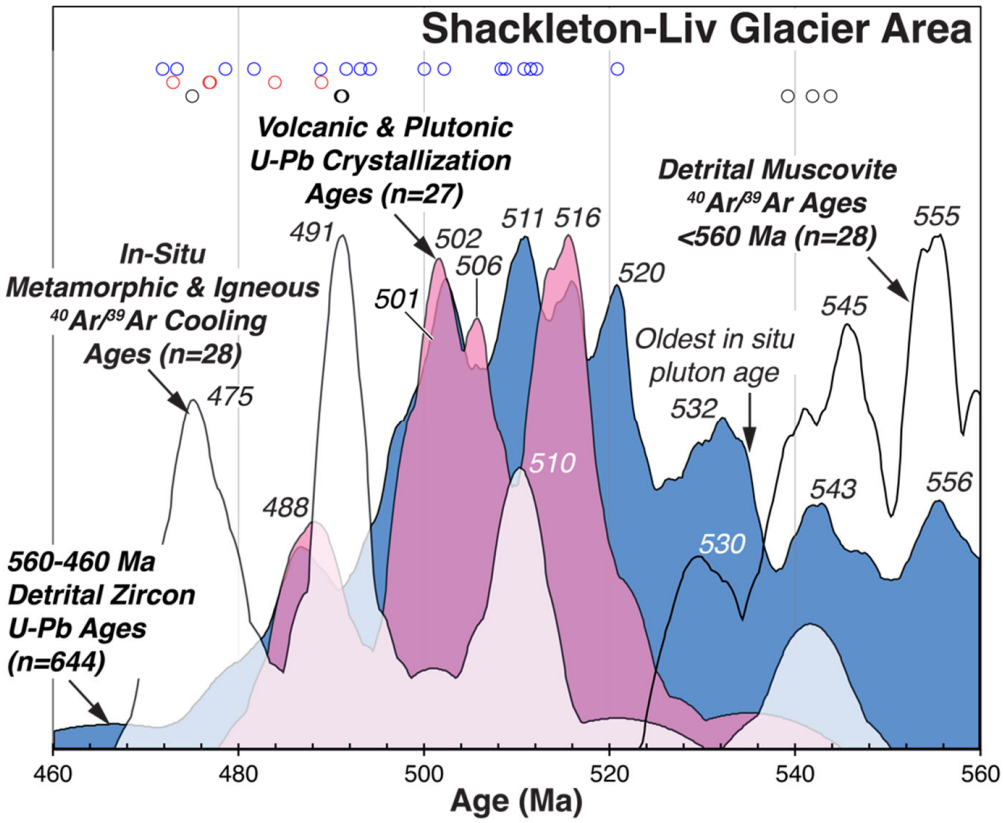

Figure 9. Stacked kernel-density-estimation diagrams [73] showing in situ igneous and metamorphic $^{40}Ar/^{39}Ar$ cooling ages, detrital zircon U-Pb ages, volcanic and plutonic U-Pb crystallization ages, and detrital muscovite $^{40}Ar/^{39}Ar$ ages falling within the 560–460 Ma time period from the Shackleton Glacier area (Ramsey to Liv glaciers) of the Ross orogen. $^{40}Ar/^{39}Ar$ age contributions from hornblende (blue circle), muscovite (red circle), and biotite (black circle) are shown above the cumulative KDE diagram for in situ igneous and metamorphic $^{40}Ar/^{39}Ar$ cooling ages. In situ igneous and metamorphic $^{40}Ar/^{39}Ar$ cooling ages are compiled from data presented in this paper, as well as [45,46,48,51,54]. Detrital zircon ages are compiled for the Liv and Beardmore groups from [26,27,54]. Volcanic and plutonic U-Pb crystallization ages are compiled from data presented in [33–36,44,45,47,48]. $^{40}Ar/^{39}Ar$ ages for detrital muscovite from the Starshot Formation along Ramsey Glacier are from [45].

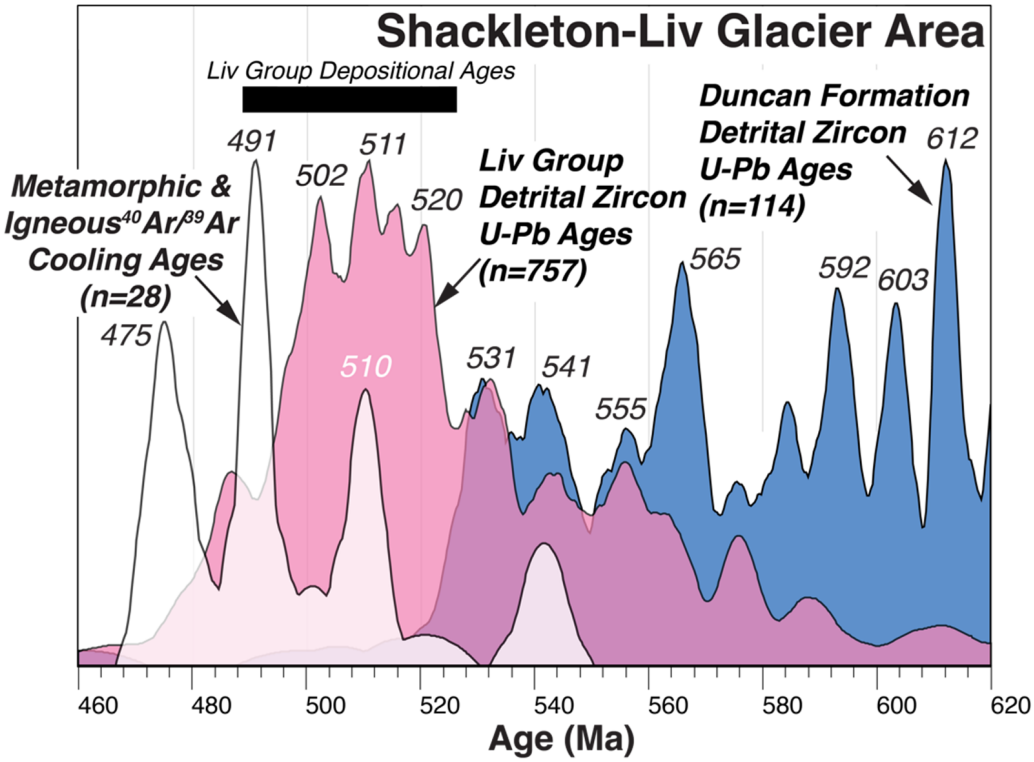

Figure 10. Stacked kernel-density-estimation diagrams [73] showing in situ igneous and metamorphic $^{40}Ar/^{39}Ar$ cooling ages, Liv Group detrital zircon U-Pb ages, and Duncan Formation detrital zircon U-Pb ages falling within the 620–460 Ma time period from the Shackleton Glacier area (Ramsey to Liv Glaciers) of the Ross orogen. In situ igneous and metamorphic $^{40}Ar/^{39}Ar$ cooling ages are compiled from data presented in this paper, as well as [45,46,48,51,54]. Detrital zircon ages are compiled for the Liv Group and Duncan Formation from [26,27,54].

The oldest (520 Ma) $^{40}Ar/^{39}Ar$ hornblende cooling age produced by our analyses on sample WSH-6B is inconsistent with U-Pb age data from the same sample [48], as well as the remaining $^{40}Ar/^{39}Ar$ age data (~510–475 Ma) reported in this paper and from previous studies in the area [45,48,51]. However, even if we accept this age, the plutonic and metasedimentary rocks of the area yield $^{40}Ar/^{39}Ar$ mineral cooling ages that are younger than, and thus are not the source of, ~555 Ma single-step single-grain detrital muscovite $^{40}Ar/^{39}Ar$ ages found in low-grade Starshot Formation sandstones located ~60 km to the west of Shackleton Glacier along Ramsey Glacier at Four Ramps (Figures 4 and 9) [54]. Detrital mica is not likely to survive long-distance fluvial or marine transport, suggesting that the ~555 Ma $^{40}Ar/^{39}Ar$ muscovite ages record igneous or metamorphic cooling in a proximal source area along the East Antarctic margin. To provide further insight into the possible source areas for this detrital mica population, we compiled and analyzed all $^{40}Ar/^{39}Ar$ cooling ages (n = 63) reported for intrusive and metamorphic rocks for the Ross orogen from south Victoria Land through the Queen Maud Mountains. The kernel density analysis in Figure 11 confirms that a significant phase of igneous and metamorphic cooling commenced at ~509 Ma within the exposed areas of the Ross orogenic belt. It also shows a general dearth of evidence for ~555 Ma cooling with the oldest 540 Ma age peak reflecting problematic and questionable biotite $^{40}Ar/^{39}Ar$ ages discussed above.

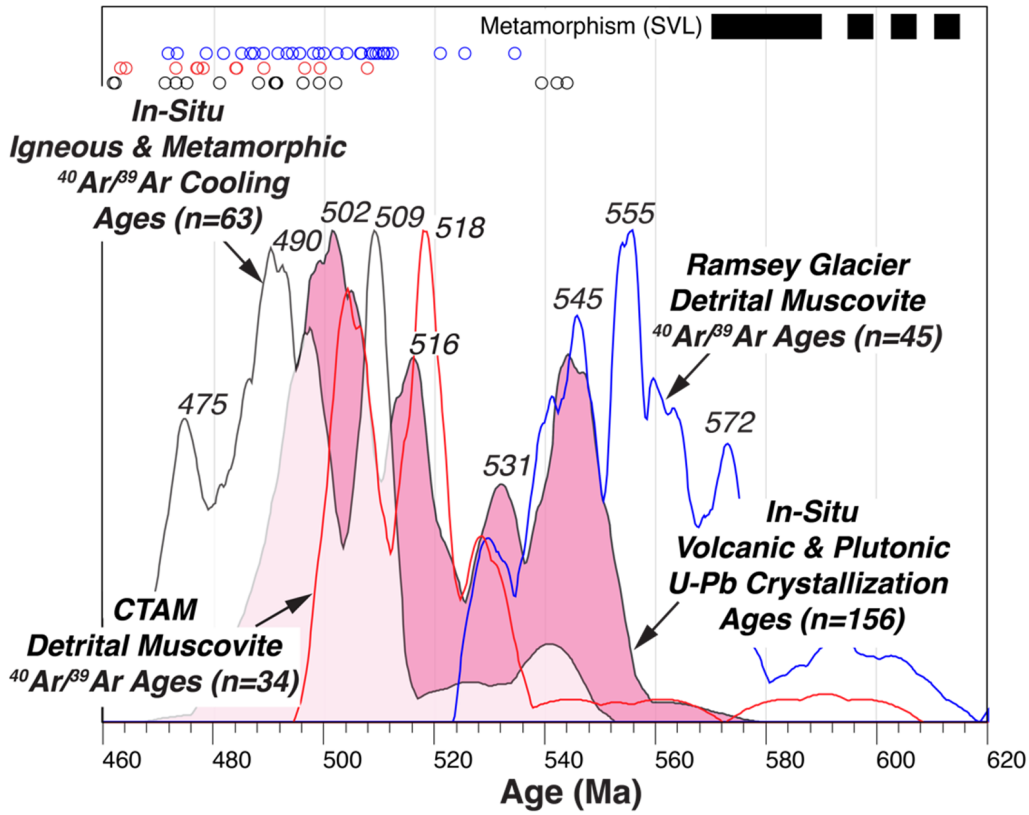

Figure 11. Stacked kernel-density-estimation diagrams [73] showing in situ igneous and metamorphic $^{40}Ar/^{39}Ar$ cooling ages and igneous U-Pb crystallization ages falling within the 620–460 Ma time period from the Queen Maud Mountains, central Transantarctic Mountains, and south Victoria Land areas of the Ross orogen. $^{40}Ar/^{39}Ar$ age contributions from hornblende (blue circle), muscovite (red circle), and biotite (black circle) are shown above the cumulative KDE diagram for in situ igneous and metamorphic $^{40}Ar/^{39}Ar$ cooling ages. In situ igneous and metamorphic $^{40}Ar/^{39}Ar$ cooling ages are compiled from data presented in this paper, as well as [37,45,46,48,51,52,54,79–83]. U-Pb crystallization ages from [33–38,44–48,82,84–99]. $^{40}Ar/^{39}Ar$ cooling ages for detrital muscovite from the Starshot Formation along Ramsey Glacier are from [54] and those within the central Transantarctic Mountains (CTAM) are from [37].

There is, however, evidence for older igneous and metamorphic bedrock along the Transantarctic Mountains area. U-Pb zircon age analyses have yielded older (565–545 Ma) igneous crystallization ages for in situ bedrock samples in the Miller Range and south Victoria Land (Figures 2, 3 and 11) [44,90,91,97,99,100]. In south Victoria Land, sandstones, pelites, and marbles belonging to the Skelton Group were deformed and experienced garnet-grade metamorphism during an early phase of presumed shortening at c. 590–570 Ma (Lu-Hf garnet) and perhaps as early as ca. 615–610 Ma (Figure 3) [101]. In addition, igneous glacial clasts recovered from the East Antarctic ice sheet in the central Transantarctic Mountains have yielded 590–554 Ma U-Pb zircon crystallization ages [99], suggesting that similar detrital zircon age populations found in siliciclastic successions along the margin may reflect the erosion of older unexposed igneous rocks in East Antarctica [11,21,54,102,103]. Detrital hornblende and apatite recovered from moraines along the Nimrod and Byrd glaciers in the central Transantarctic Mountains show 640–450 Ma $^{40}Ar/^{39}Ar$ and apatite U-Pb (similar to hornblende closure temperature) cooling ages [104]. Detrital muscovite grains recovered from glacial tills along one glacial drainage (Byrd Glacier) have yielded younger 531–473 $^{40}Ar/^{39}Ar$ ages [105], which are similar to detrital muscovite $^{40}Ar/^{39}Ar$ ages found in low-grade Starshot Formation sandstones in the central Transantarctic Mountains [37]. Thus, the collective evidence suggests that the ~555 Ma $^{40}Ar/^{39}Ar$ muscovite cooling ages in the Ramsey Glacier area probably reflect

the erosion of proximal unidentified or unexposed (ice-covered) igneous or metamorphic source areas with older cooling histories located inboard of the Transantarctic Mountains in East Antarctica.

Attributing detrital minerals to the erosion of older sectors of the orogenic belt has merit because it can account for the source of siliciclastic successions that appear to have been deposited prior to the onset of Liv Group volcanism and subsequent < 510 Ma igneous and metamorphic cooling (Figure 3). In the Liv Glacier area, the Duncan Formation is comprised of quartzites and schists, along with minor interbedded marbles, but is devoid of interbedded volcanic rocks [24,41,63]. In the Duncan Mountains, the Duncan Formation is juxtaposed against the Fairweather Formation (Liv Group) along the Spillway Fault (Figures 4 and 12), with shear sense indicators, implying that the Duncan Formation is thrust on to the Fairweather and is therefore stratigraphically lower and older than the Fairweather Formation [24]. Detrital zircon U-Pb age analyses from two Duncan Formation samples have yielded significant populations of ~630–530 Ma zircons with age peaks (549 Ma and 539 Ma) providing firm maximum depositional age limits (Figures 8A and 9) for the Duncan Formation [27,54]. The 477 Ma $^{40}Ar/^{39}Ar$ muscovite plateau cooling age from the Duncan Formation schist sample AOG is similar to 477–475 Ma white mica and phlogopite $^{40}Ar/^{39}Ar$ plateau metamorphic cooling ages for Fairweather Formation metasandstones collected at Mt. Henson (Figure 8A, Table S1) [51]. These data indicate regional metamorphic cooling across the Spillway Fault through the muscovite closure temperature (~450 °C [69]) by 477 Ma and provide a new minimum age for the deposition of the Duncan Formation. Collectively, the age relations place the deposition of the Duncan Formation within the Cambrian (Terreneuvian) to Lower Ordovician (539–477 Ma) time interval (Figure 8A) but likely prior to the local deposition of the Liv Group.

Figure 12. Photo of isoclinally folded Henson Marble Member of the Fairweather Formation in structural contact with the Duncan Formation along the Spillway Fault at Mount Henson.

The 477 Ma $^{40}Ar/^{39}Ar$ metamorphic cooling age for sample AOG rules out correlation of the Duncan Formation with younger Lower to Middle Ordovician flysch deposits such as those found along the Lachlan orogen in Australia that have been related to the unroofing of the Ross orogen [106]. Instead, the Duncan Formation belongs to a suite of late Neoproterozoic to Cambrian siliciclastic rocks found in the Queen Maud Mountains (Figure 3). Samples of the La Gorce Formation yielded ~600–580 Ma detrital zircons that

are, in broad terms, similar to detrital zircon age populations yielded by the Duncan Formation [26,27,54]. Samples mapped as the La Gorce Formation from the Reedy Glacier area possess young (~537–524 Ma) maximum depositional ages [27], the youngest of which suggests deposition during the 526–489 Ma record of Liv Group volcanism. However, La Gorce Formation sandstones from the upper Scott and Amundsen glaciers yielded older (~605–580 Ma) maximum depositional ages [26,27] and are locally cross-cut by ~526 Ma hypabyssal intrusive rocks of the Wyatt Formation (Liv Group) [26,44,107]. Thus, parts of the Duncan and La Gorce formations may represent synorogenic flysch derived from the erosion of older elements of the Ross orogen. If this is the case, then it raises the question as to why tectonothermal activity subsequently migrated to this outboard region. Insight into this issue comes from an examination of geologic data from along the range to which we now turn.

Chemical and isotopic studies of bimodal volcanic rocks belonging to the Liv Group suggest volcanism occurred within an extensional rift environment [32]. Bimodal volcanic rocks belonging to the Liv Group include dacites, rhyolites, and volumetrically minor basalts and basaltic andesites [32,63]. Trace element and Sr-Nd isotopic signatures suggest that felsic rocks involved melting continental crust and fractionation of mafic melts, whereas the mafic rocks appear to be derived from melting of asthenospheric mantle [32]. The widespread emplacement of calk-alkaline granitoids (i.e., the Granite Harbor intrusive suite) during the Cambrian (the same time period as Liv Group deposition) suggests that the Ross orogeny was related to subduction [35,73]. Thus, the evidence suggests deposition of the Liv Group within an extensional rift environment, likely within an intra-arc or back-arc basin [32]. In the Queen Maud Mountains, this volcanism and associated intrusive activity followed an earlier phase of deformation involving La Gorce Formation that is bracketed within the 581–526 Ma time interval [26,44,107].

Tectonothermal activity is likely to have varied in space and time along the Ross orogenic belt. However, in the central Transantarctic Mountains at the Miller Range, U-Pb analyses yielded a ~536 Ma age for high-pressure (16–18 kbar) eclogite facies metamorphism (Figure 3), followed by rapid decompression to mid-crustal depths (8–10 kbar) by 525 Ma that has been attributed to exhumation during crustal extension [108]. In South Victoria Land, Skelton Group sedimentary rocks experienced an intermediate pressure (5.6–7.8 kbar) metamorphism attributed to an early phase of crustal thickening (>540 Ma), followed by decompression to lower-pressure conditions (1.7–5,3 kbar) by ~505 Ma [109]. Skelton Group metasedimentary rocks have yielded ~590–570 Ma Lu-Hf ages for garnet-grade metamorphism attributed to the early phase of crustal thickening, which was followed by ~550–525 Ma alkaline magmatism that has also, in turn, been attributed to crustal extension [91,101]. In both of these cases, crustal extension was followed by the introduction of voluminous magmatism in the outboard, presently exposed sectors of the Ross orogen (Figure 13) [44]. One explanation for these correlations is that they mark a change in plate boundary conditions along the East Antarctic margin, for example, with early contraction, followed by upper plate extension and outboard directed arc migration induced by slab rollback and steepening during subduction (Figure 14) [44,110].

According to standard models, slab rollback relative to the upper plate could cause rifting of the upper plate and migration of arc magmatism with the trench to a more outboard position [111]. Thus, slab rollback may occur in association with a decrease in crustal thickness due to upper plate extension [110]. Magmas resulting from rifting or arc magmatism through thinner outboard (forearc) crust have the potential to record the change in crustal thickness in their zircon chemistry. Trace elements in zircon can been used to understand the tectonic conditions in which they formed within their magma chambers and potential changes that have occurred over time [112]. Garnet is a mineral whose presence in magmas is sensitive to pressure, garnet being stable at higher pressures. Garnet incorporates heavy rare-earth elements (HREEs) and Yb relative to other trace elements [113]. Therefore, changes in Yb/Gd ratios in zircon crystallizing in the presence or absence of garnet, for example, are thought to correlate with changes in crustal thickness

during magmatism [112]. To evaluate crustal thickness patterns over the 620–460 Ma time interval, we analyzed the trace element record retained within detrital zircons from sandstones collected from the Queen Maud Mountains to south Victoria Land [27,114].

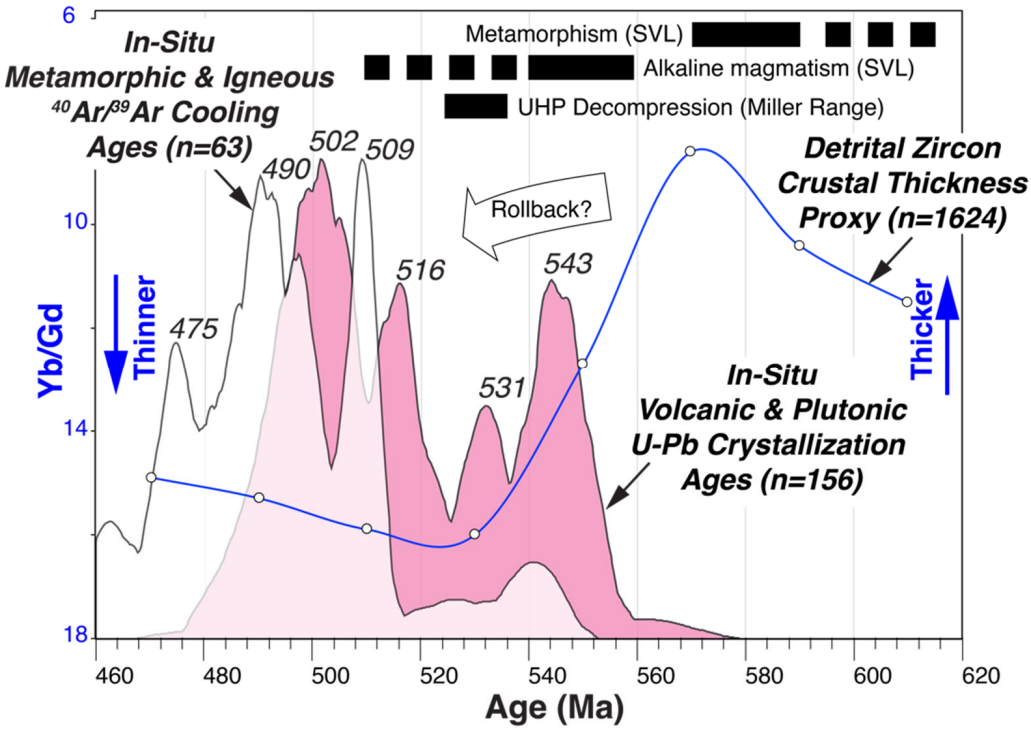

Figure 13. Average detrital zircon Yb/Gd ratios (20 Myr time brackets) with respect to the timing of metamorphism associated with crustal thickening in south Victoria Land [101], alkaline volcanism in south Victoria Land [91], and decompression of ultra-high-pressure metamorphic rocks in the central Transantarctic Mountains [108], as well as stacked kernel-density-estimation diagrams [73] showing in situ igneous and metamorphic $^{40}Ar/^{39}Ar$ cooling ages and igneous U-Pb crystallization ages falling within the 620–460 Ma time period in the Ross orogenic belt from South Victoria Land through the Queen Maud Mountains. Note that the zircon Yb/Gd ratio decreases upwards correlating with increasing crustal thickness. Detrital zircon Yb/Gd data include all zircons regardless of concordance with Th/U > 0.1 (~igneous proxy) and Th, U, Y, Yb, and Gd values > 0. Interpreted zircon ages are $^{206}Pb/^{238}U$ ages for grains with $^{206}Pb/^{207}Pb$ ages < 1500 Ma. $^{40}Ar/^{39}Ar$ cooling ages are compiled from data presented in this paper, as well as [37,45,46,48,51,52,54,79–83]. U-Pb igneous crystallization ages are presented in [33–38,44–48,82,84–99].

The zircon age and trace element data show that the lowest average Yb/Gd ratios indicative of thicker crust correlate with the ~580–560 Ma time interval (Figure 13), which overlaps with metamorphic Lu-Hf garnet ages correlated with crustal thickening in south Victoria Land [101]. These lower ratios are followed by a pronounced ~560–530 Ma increase in Yb/Gd values indicative of magmatism within thinner crust. Detrital zircon trace element patterns for sandstones along the north Victoria Land sector of the orogen record a similar change in crustal thickness during this same time period [11]. This change in crustal thickness retained within the detrital zircon archive correlates with other evidence of extension during this interval as discussed above, as well as the appearance of voluminous magmatism in outboard locations along the margin (Figure 13). We therefore suggest that the ~510 Ma episode of igneous and metamorphic cooling soon after igneous crystallization in the Queen Maud Mountains is likely due to the emplacement of magmas in thinner extended or extending crust as the locus of arc magmatism induced by slab rollback shifted outboard during the Ross orogeny (Figure 14). Volcanic, siliciclastic, and carbonate sequences were emplaced along the Transantarctic Mountains during this phase. Collectively, these changes along the margin overlap with the ~590–550 collision of

East-West Gondwana along the Mozambique orogenic belt [2,3,9,115], suggesting that they coincided with possible global plate motion changes induced during the final assembly of Gondwana.

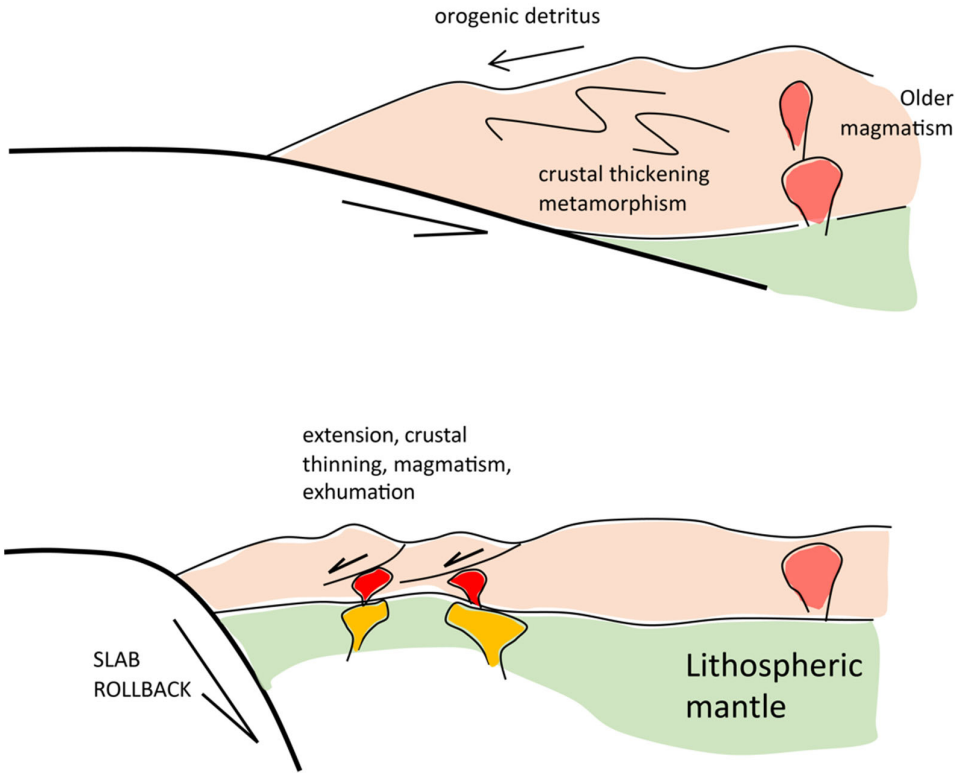

Figure 14. Schematic tectonic model for the Queen Maud Mountain–south Victoria Land sector of the paleo-Pacific margin of Gondwana. The upper figure broadly corresponds to the earlier time (~late Neoproterozoic-early Cambrian) of crustal thickening indicated in Figure 13, whereas the lower figure corresponds to the later time (~Cambrian) of crustal thinning, possibly due to extension related to slab rollback.

On a regional scale, there is a similarity in the orogenic history of the Ross orogeny recorded in the Transantarctic Mountains to other areas along Gondwana's paleo-Pacific margin. Widespread deposition of siliciclastic, carbonate, and in some cases, volcanic successions, occurred along Gondwana's margin in the Cambrian. Deposition of such sequences has been interpreted to have occurred in extensional basins in South Africa [116], the Ellsworth Mountains [117,118], and the Pensacola Mountains [119,120], as well as in north Victoria Land, Tasmania, and Australia [116,121]. In South Africa and the Pensacola Mountains, these successions overlie unconformities developed during earlier Neoproterozoic to early Cambrian deformation considered to represent the main orogenic episode in these regions [116,122]. Deformation of these Cambrian sequences is weak to absent in South Africa, the Ellsworth Mountains, and the Pensacola Mountains [117,118]. This is unlike many of the successions farther along the margin, such as those in the outboard localities of the Transantarctic Mountains, which experienced higher degrees of subsequent middle to late Cambrian horizontal shortening that led to the structural suites that have long been considered the defining expression of the Ross orogeny [17,41].

6. Conclusions

Our $^{40}Ar/^{39}Ar$ results constrain igneous and metamorphic cooling to have occurred as early as ~510 Ma in the Shackleton–Liv Glacier area of the Queen Maud Mountains. Igneous and metamorphic cooling commenced following the onset of magmatism in the area. These results are consistent with igneous and metamorphic cooling ages found

elsewhere within the Ross orogen. The new data further demonstrate the widespread onset of tectonothermal activity in the outboard portions of the Ross orogenic belt in the Cambrian. These results, along with others, can be interpreted to support a late Neoproterozoic to Cambrian (Terreneuvian) shortening and thickening event associated with the final stages of Gondwana assembly. This was followed by a change in plate motions along the paleo-Pacific margin that initiated a short-lived Cambrian extensional and crustal thinning event due to slab rollback. Intrusions, arc-related volcanics, and carbonate sequences were emplaced along the Transantarctic Mountains and other parts of the paleo-Pacific margin of Gondwana. Subsequent shortening during the Cambrian to Ordovician led to changes in sedimentation patterns [22], as well as supracrustal deformation that typifies the Ross orogeny in outboard regions [17,41]. Our results invite further work to address the broader tectonic factors that caused these events.

Supplementary Materials: The following are available online at https://www.mdpi.com/article/10.3390/geosciences13040126/s1, Figure S1: $^{40}Ar/^{39}Ar$ incremental release spectra; Figure S2: Photographs of metasedimentary, foliated/pretectonic, and unfoliated intrusive rock samples; Table S1: $^{40}Ar/^{39}Ar$ ages and analytical data for samples from the Shackleton–Liv Glacier area, Transantarctic Mountains, Antarctica; Table S2: Analytical Data.

Author Contributions: Conceptualization, T.P. and J.E.; methodology, T.P., J.E., J.B. and P.L.; software, T.P.; writing—original draft preparation, T.P. and J.E.; writing—review and editing, T.P., J.E., A.G., J.B., P.L., C.D. and J.S.; funding acquisition, A.G. and T.P. All authors have read and agreed to the published version of the manuscript.

Funding: This research was funded by the University of Wisconsin Oshkosh Faculty Development Program, grant number FDR1296.

Data Availability Statement: The data reported here are available in the Supplementary Files that accompany this manuscript.

Acknowledgments: This research was supported by NSF grant OPP-9317673 to A. Grunow, NSF grant OPP-0835480 to T. Paulsen, NSF grant OPP-9726104 to J. Encarnación and the University of Wisconsin Oshkosh Faculty Development Program. The rock samples were provided the Polar Rock Repository with support from the National Science Foundation, under Cooperative Agreement OPP-2137467. DOI: https://doi.org/10.7289/V5RF5S18 (accessed on: 17 February 2023.). Fieldwork was supported by the Office of Polar Programs, U.S. National Science Foundation. We thank Michel Villeneuve and two anonymous reviewers for helpful feedback that improved this manuscript, as well as Mike Roberts for his assistance in the field.

Conflicts of Interest: The authors declare no conflict of interest.

References

1. Wilson, J.T. Did the Atlantic Close and Then Reopen? *Nature* **1966**, *211*, 676–681. [CrossRef]
2. Grunow, A.M.; Hanson, R.; Wilson, T. Were Aspects of Pan-African Deformation Linked to Iapetus Opening? *Geology* **1996**, *24*, 1063–1066. [CrossRef]
3. Squire, R.J.; Campbell, I.H.; Allen, C.M.; Wilson, C.J.L. Did the Transgondwanan Supermountain Trigger the Explosive Radiation of Animals on Earth? *Earth Planet. Sci. Lett.* **2006**, *250*, 116–133. [CrossRef]
4. Brown, M. Metamorphic Conditions in Orogenic Belts: A Record of Secular Change. *Int. Geol. Rev.* **2007**, *49*, 193–234. [CrossRef]
5. Hawkesworth, C.; Cawood, P.; Kemp, T.; Storey, C.; Dhuime, B. Geochemistry. A Matter of Preservation. *Science* **2009**, *323*, 49–50. [CrossRef] [PubMed]
6. Condie, K.C.; Aster, R.C. Episodic Zircon Age Spectra of Orogenic Granitoids: The Supercontinent Connection and Continental Growth. *Precambrian Res.* **2010**, *180*, 227–236. [CrossRef]
7. Ganade De Araujo, C.E.; Rubatto, D.; Hermann, J.; Cordani, U.G.; Caby, R.; Basei, M.A.S. Ediacaran 2,500-Km-Long Synchronous Deep Continental Subduction in the West Gondwana Orogen. *Nat. Commun.* **2014**, *5*, 5198. [CrossRef]
8. Cawood, P.A.; Martin, E.L.; Murphy, J.B.; Pisarevsky, S.A. Gondwana's Interlinked Peripheral Orogens. *Earth Planet. Sci. Lett.* **2021**, *568*, 117057. [CrossRef]
9. Boger, S.D.; Miller, J.M. Terminal Suturing of Gondwana and the Onset of the Ross-Delamerian Orogeny: The Cause and Effect of an Early Cambrian Reconfiguration of Plate Motions. *Earth Planet. Sci. Lett.* **2004**, *219*, 35–48. [CrossRef]
10. Cohen, K.M.; Finney, S.C.; Gibbard, P.L.; Fan, J.-X. The ICS International Chronostratigraphic Chart. *Episodes* **2013**, *36*, 199–204. [CrossRef]

11. Paulsen, T.S.; Deering, C.; Sliwinski, J.; Bachmann, O.; Guillong, M. A Continental Arc Tempo Discovered in the Pacific-Gondwana Margin Mudpile? *Geology* **2016**, *44*, 915–918. [CrossRef]
12. Domeier, M.; Torsvik, T.H. Plate Tectonics in the Late Paleozoic. *Geosci. Front.* **2014**, *5*, 303–350. [CrossRef]
13. Goodge, J.W. Geological and Tectonic Evolution of the Transantarctic Mountains, from Ancient Craton to Recent Enigma. *Gondwana Res.* **2020**, *80*, 50–122. [CrossRef]
14. Isbell, J.L.J.L. The Kukri Erosion Surface; a Reassessment of Its Relationship to Rocks of the Beacon Supergroup in the Central Transantarctic Mountains, Antarctica. *Antarct. Sci* **1999**, *11*, 228–238. [CrossRef]
15. Stump, E. *The Ross Orogen of the Transantarctic Mountains*; Cambridge University Press: Cambridge, UK, 1995.
16. Mirsky, A. *Geology of the Ohio Range–Liv Glacier Area*; Antarctic Map Folio Series (Folio 12, Plate 16); American Geographical Society: New York, NY, USA, 1969.
17. Grindley, G.W.; McDougall, I. Age and Correlation of the Nimrod Group and Other Precambrian Rock Units in the Central Transantarctic Mountains, Antarctica. *N. Z. J. Geol. Geophys.* **1969**, *12*, 391–411. [CrossRef]
18. McGregor, V.R.; Wade, F.A. *Geology of the Western Queen Maud Mountains*; Antarctic Map Folio Series (Folio 12, Plate 15); American Geographical Society: New York, NY, USA, 1969.
19. Warren, G. *Geology of the Terra Nova Bay-McMurdo Sound Area, Victoria Land*; Antarctic Map Folio Series (Folio 12, Plate 13); American Geographical Society: New York, NY, USA, 1969.
20. Davis, M.B.; Blankenship, D.D. *Geology of the Scott-Reedy Glaciers Area Southern Transantarctic Mountains, Antarctica*; Geological Society of America: Boulder, CO, USA, 2005. [CrossRef]
21. Goodge, J.W.; Williams, I.S.; Myrow, P. Provenance of Neoproterozoic and Lower Paleozoic Siliciclastic Rocks of the Central Ross Orogen, Antarctica: Detrital Record of Rift-, Passive-, and Active-Margin Sedimentation. *Geol. Soc. Am. Bull.* **2004**, *116*, 1253–1279. [CrossRef]
22. Myrow, P.M.; Pope, M.C.; Goodge, J.W.; Fischer, W.; Palmer, A.R. Depositional History of Pre-Devonian Strata and Timing of Ross Orogenic Tectonism in the Central Trananarctic Mountains, Antarctica. *Bull. Geol. Soc. Am.* **2002**, *114*, 1070–1088. [CrossRef]
23. Laird, M.G.; Mansergh, G.D.; Chappell, J.M.A. Geology of the Central Nimrod Glacier Area, Antarctica. *N. Z. J. Geol. Geophys.* **1971**, *14*, 427–468. [CrossRef]
24. Stump, E. Structural Relationships in the Duncan Mountains, Central Transantarctic Mountains, Antarctica. *N. Z. J. Geol. Geophys.* **1981**, *24*, 87–93. [CrossRef]
25. Stump, E. The Ross Supergroup in the Queen Maud Mountains. In *Antarctic Geoscience*; Craddock, C., Ed.; University of Wisconsin Press: Madison, WI, USA, 1982; pp. 565–569.
26. Stump, E.; Gehrels, G.; Talarico, F.; Carosi, R. Constraints from Detrital Zircon Geochronology on the Early Deformation of the Ross Orogen, Transantarctic Mountains, Antarctica, in Antarctica: A Keystone in a Changing World. In *Proceedings of the 10th International Symposium on Antarctic Earth Sciences, Santa Barbara, CA, USA, 26 August–1 September 2007*; Cooper, A.K., Raymond, C.R., Eds.; USGS Open-File Report 2007-1047, Extended Abstract 166; The National Academies Press: Washington, DC, USA, 2007; 3p.
27. Paulsen, T.S.; Deering, C.; Sliwinski, J.; Bachmann, O.; Guillong, M. Evidence for a Spike in Mantle Carbon Outgassing during the Ediacaran Period. *Nat. Geosci.* **2017**, *10*, 930–933. [CrossRef]
28. Goodge, J.W.; Myrow, P.; Williams, I.S.; Bowring, S.A. Age and Provenance of the Beardmore Group, Antarctica: Constraints on Rodinia Supercontinent Breakup. *J. Geol.* **2002**, *110*, 393–406. [CrossRef]
29. Cooper, A.F.; Maas, R.; Scott, J.M.; Barber, J.W. Dating of Volcanism and Sedimentation in the Skelton Group, Transantarctic Mountains: Implications for the Rodinia- Gondwana Transition in Southern Victoria Land, Antarctica. *Bull. Geol. Soc. Am.* **2011**, *123*, 681–702. [CrossRef]
30. Rowell, A.J.; Rees, M.N. Early Palaeozoic History of the Upper Beardmore Glacier Area: Implications for a Major Antarctic Structural Boundary within the Transantarctic Mountains. *Antarct. Sci.* **1989**, *1*, 249–260. [CrossRef]
31. Rowell, A.J.; Gonzales, D.A.; McKenna, L.W.; Evans, K.R.; Stump, E.; van Schmus, W.R. Lower Paleozoic Rocks in the Queen Maud Mountains: Revised Ages and Significance. In *The Antarctic Region: Geological Evolution and Processes*; Terra Antarctica Publication: Siena, Italy, 1997; pp. 201–207.
32. Wareham, C.D.; Stump, E.; Storey, B.C.; Millar, I.L.; Riley, T.R. Petrogenesis of the Cambrian Liv Group, a Bimodal Volcanic Rock Suite from the Ross Orogen, Transantarctic Mountains. *Bull. Geol. Soc. Am.* **2001**, *113*, 360–372. [CrossRef]
33. Encarnación, J.; Rowell, A.J.; Grunow, A.M. A U-Pb Age for the Cambrian Taylor Formation, Antarctica: Implications for the Cambrian Time Scale. *J. Geol.* **1999**, *107*, 497–504. [CrossRef]
34. van Schmus, W.R.; McKenna, L.W.; Gonzales, D.A.; Fetter, A.H.; Rowell, A.J. U-Pb Geochronology of Parts of the Pensacola, Thiel, and Queen Maud Mountains, Antarctica. In *The Antarctic Region: Geological Evolution and Processes*; Terra Antarctica Publication: Siena, Italy, 1997; pp. 187–200.
35. Paulsen, T.S.; Encarnación, J.; Grunow, A.M.; Stump, E.; Pecha, M.; Valencia, V.A. Correlation and Late-Stage Deformation of Liv Group Volcanics in the Ross-Delamerian Orogen, Antarctica, from New U-Pb Ages. *J. Geol.* **2018**, *126*, 307–323. [CrossRef]
36. Paulsen, T.S.; Encarnación, J.; Grunow, A.; Pecha, M. Zircon U–Pb Age Constraints for a Cambrian Age for Metasedimentary Rocks at O'Brien Peak, Antarctica. *N. Z. J. Geol. Geophys.* **2016**, *59*, 592–597. [CrossRef]
37. Goodge, J.W.; Myrow, P.; Phillips, D.; Fanning, C.M.; Williams, I.S. Siliciclastic Record of Rapid Denudation in Response to Convergent-Margin Orogenesis, Ross Orogen, Antarctica. *Spec. Pap. Geol. Soc. Am.* **2004**, *378*, 105–126. [CrossRef]

38. Stump, E.; Gootee, B.F.; Talarico, F.; Van Schmus, W.R.; Brand, P.K.; Foland, K.A.; Fanning, C.M. Correlation of Byrd and Selborne Groups, with Implications for the Byrd Glacier Discontinuity, Central Transantarctic Mountains, Antarctica. *N. Z. J. Geol. Geophys.* **2004**, *47*, 157–171. [CrossRef]
39. Murtaugh, J.G. Geology of the Wisconsin Range Batholith, Transantarctic Mountains. *N. Z. J. Geol. Geophys.* **1969**, *12*, 526–550. [CrossRef]
40. Borg, S.G.; DePaolo, D.J.; Smith, B.M. Isotopic Structure and Tectonics of the Central Transantarctic Mountains. *J. Geophys. Res. Solid Earth* **1990**, *95*, 6647–6667. [CrossRef]
41. McGregor, V.R. Geology of the Area Between the Axel Heiberg and Shackleton Glaciers, Queen Maud Range, Antarctica: Part I-Basement Complex, Structure, and Glacial Geology. *N. Z. J. Geol. Geophys.* **1965**, *8*, 314–343. [CrossRef]
42. Borg, S.G.; DePaolo, D.J. A Tectonic Model of the Antarctic Gondwana Margin with Implications for Southeastern Australia: Isotopic and Geochemical Evidence. *Tectonophysics* **1991**, *196*, 339–358. [CrossRef]
43. Borg, S.G.; DePaolo, D.J. Laurentia, Australia, and Antarctica as a Late Proterozoic Supercontinent. Constraints from Isotopic Mapping. *Geology* **1994**, *22*, 307–310. [CrossRef]
44. Encarnación, J.; Grunow, A. Changing Magmatic and Tectonic Styles along the Paleo-Pacific Margin of Gondwana and the Onset of Early Paleozoic Magmatism in Antarctica. *Tectonics* **1996**, *15*, 1325–1341. [CrossRef]
45. Paulsen, T.S.; Encarnación, J.; Grunow, A.M.; Valencia, V.A.; Pecha, M.; Layer, P.W.; Rasoazanamparany, C. Age and Significance of "outboard" High-Grade Metamorphics and Intrusives of the Ross Orogen, Antarctica. *Gondwana Res.* **2013**, *24*, 349–358. [CrossRef]
46. Paulsen, T.; Encarnación, J.; Grunow, A.; Valencia, V.A.; Rasoazanamparany, C. Late Sinistral Shearing along Gondwana's Paleo-Pacific Margin in the Ross Orogen, Antarctica: New Structure and Age Data from the O'Brien Peak Area. *J. Geol.* **2008**, *116*, 303–312. [CrossRef]
47. Vogel, M.B.; Ireland, T.R.; Weaver, S.D. The Multistage History of the Queen Maud Batholith, La Gorce Mountains, Central Transantarctic Mountains. In *Antarctica at the Close of a Millennium, Proceedings of the 8th International Symposium on Antarctic Earth Sciences, Wellington, 5–9 July 1999*; Royal Society of New Zealand: Wellington, New Zealand, 2002; pp. 153–159.
48. Paulsen, T.; Encarnación, J.; Grunow, A.M.; Valencia, V.A.; Pecha, M.E.; Benowitz, J.; Layer, P. New Ages from the Shackleton Glacier Area and Their Context in the Regional Tectonomagmatic Evolution of the Ross Orogen of Antarctica. *Int. Geol. Rev.* **2020**, *63*, 1596–1618. [CrossRef]
49. Felder, R.P.; Faure, G. Investigation of an Anomalous Date for Lonely Ridge Granodiorite, Nilsen Plateau, Transantarctic Mountains. *Antarct. J. U.S.* **1979**, *14*, 24.
50. Faure, G.; Eastin, R.; Ray, P.T.; Mclelland, D.; Shultz, C.H. *Geochronology of Igneous and Metamorphic Rocks, Central Transantarctic Mountains*; Raja Rao, C.S., Ed.; Hindustan Publishing Corporation: Calcutta, India, 1979.
51. Paulsen, T.S.; Encarnación, J.; Grunow, A.M. Structure and Timing of Transpressional Deformation in the Shackleton Glacier Area, Ross Orogen, Antarctica. *J. Geol. Soc. Lond.* **2004**, *161*, 1027–1038. [CrossRef]
52. Grunow, A.M.; Encarnación, J. Terranes or Cambrian Polar Wander: New Data from the Scott Glacier Area, Transantarctic Montains, Antarctica. *Tectonics* **2000**, *19*, 168–181. [CrossRef]
53. Grunow, A.M.; Encarnación, J.P. Cambro-Ordovician Palaeomagnetic and Geochronologic Data from Southern Victoria Land, Antarctica: Revision of the Gondwana Apparent Polar Wander Path. *Geophys. J. Int.* **2000**, *141*, 392–400. [CrossRef]
54. Paulsen, T.S.; Encarnación, J.; Grunow, A.M.; Valencia, V.A.; Layer, P.W.; Pecha, M.; Stump, E.; Roeske, S.; Thao, S.; Rasoazanamparany, C. Detrital Mineral Ages from the Ross Supergroup, Antarctica: Implications for the Queen Maud Terrane and Outboard Sediment Provenance on the Gondwana Margin. *Gondwana Res.* **2015**, *27*, 377–391. [CrossRef]
55. Samson, S.D.; Alexander, E.C. Calibration of the Interlaboratory 40Ar/39Ar Dating Standard, MMhb1. *Chem. Geol.* **1987**, *66*, 27–34.
56. Renne, P.R. Intercalibration of Astronomical and Radioisotopic Time. *Geology* **1994**, *22*, 783–786. [CrossRef]
57. York, D.; Hall, C.M.; Yanase, Y.; Hanes, J.A.; Kenyon, W.J. 40Ar/39Ar Dating of Terrestrial Minerals with a Continuous Laser. *Geophys. Res. Lett.* **1981**, *8*, 1136–1138. [CrossRef]
58. Layer, P.W.; Hall, C.M.; York, D. The Derivation of 40Ar/39Ar Age Spectra of Single Grains of Hornblende and Biotite by Laser Step Heating. *Geophys. Res. Lett.* **1997**, *14*, 757–760. [CrossRef]
59. Layer, P.W. Argon-40/Argon-39 Age of the El'gygytgyn Impact Event, Chukotka, Russia. *Meteorit. Planet. Sci.* **2000**, *35*, 591–599. [CrossRef]
60. Benowitz, J.A.; Layer, P.W.; Vanlaningham, S. Persistent Long-Term (c. 24 Ma) Exhumation in the Eastern Alaska Range Constrained by Stacked Thermochronology. *Geol. Soc. Lond. Spec. Publ.* **2014**, *378*, 225–243. [CrossRef]
61. McDougall, I.; Harrison, T.M. *Geochronology and Thermochronology by the 40Ar/39Ar Method*, 2nd ed.; Oxford University Press: New York, NY, USA, 1991.
62. Renne, P.R.; Mundil, R.; Balco, G.; Min, K.; Ludwig, K.R. Joint Determination of 40K Decay Constants and 40Ar∗/40K for the Fish Canyon Sanidine Standard, and Improved Accuracy for 40Ar/39Ar Geochronology. *Geochim. Cosmochim. Acta* **2010**, *74*, 5349. [CrossRef]
63. Stump, E. Stratigraphy of the Ross Supergroup, Central Transantarctic Mountains. In *Geology of the Central Transantarctic Mountains*; American Geophysical Union: Washington, DC, USA, 1986; pp. 225–274. ISBN 9781118664797.

64. Burgener, J.D. Petrography of the Queen Maud Batholith, Central Transantarctic Mountains, Ross Dependency, Antarctica. Master's Thesis, University of Wisconsin Madison, Madison, WI, USA, 1975.
65. Baldwin, S.L.; Fitzgerald, P.G.; Li, B.; Miller, S.R. Thermal Evolution of the Transantarctic Mountains in the Shackleton Glacier Area. In *Antarctica at the Close of a Millennium, Proceedings of the 8th International Symposium on Antarctic Earth Sciences, Wellington, 5–9 July 1999*; Programme and Abstracts; Skinner, D.N.B., Ed.; Royal Society of New Zealand: Wellington, New Zealand, 1999; p. 33.
66. Gaber, I.J.; Foland, K.A.; Corbato, C.E. On the Significance of Ar Release from Biotite and Amphibole during 40Ar/39Ar Vacuum Heating. *Geochim. Cosmochim. Acta* **1988**, *52*, 2457–2465. [CrossRef]
67. Brownlee, S.J.; Renne, P.R. Thermal History of the Ecstall Pluton from 40Ar/39Ar Geochronology and Thermal Modeling. *Geochim. Cosmochim. Acta* **2010**, *74*, 4375–4391. [CrossRef]
68. Harrison, M.T. Diffusion of 40Ar in Hornblende. *Contrib. Mineral. Petrol.* **1982**, *78*, 324–331. [CrossRef]
69. Dodson, M.H. Theory of Cooling Ages. In *Lectures in Isotope Geology*; Jager, E., Hunziker, H.C., Eds.; Springer Science & Business Media: Berlin, Germany, 1979; pp. 194–202.
70. Blanckenburg, F.V.; Villa, I.M.; Baur, H.; Morteani, G.; Steiger, R.H. Time Calibration of a P–T Path from the Tauern Window Eastern Alps: The Problem of Closure Temperature. *Contrib. Mineral. Petrol.* **1989**, *101*, 1–11. [CrossRef]
71. Miller, S.R.; Fitzgerald, P.G.; Baldwin, S.L. Cenozoic Range-Front Faulting and Development of the Transantarctic Mountains near Cape Surprise, Antarctica: Thermochronologic and Geomorphologic Constraints. *Tectonics* **2010**, *29*, 1–21. [CrossRef]
72. He, J.; Thomson, S.N.; Reiners, P.W.; Hemming, S.R.; Licht, K.J. Rapid Erosion of the Central Transantarctic Mountains at the Eocene-Oligocene Transition: Evidence from Skewed (U-Th)/He Date Distributions near Beardmore Glacier. *Earth Planet. Sci. Lett.* **2021**, *567*, 117009. [CrossRef]
73. Vermeesch, P. On the Visualisation of Detrital Age Distributions. *Chem. Geol.* **2012**, *312–313*, 190–194. [CrossRef]
74. Grunow, A.; Encarnación, J.P.; Paulsen, T.S.; Rowell, A.J. New Geologic Constraints on Basement Rocks from the Shackleton Glacier Region. *Antarct. J. U.S.* **1996**, *31*, 18–19.
75. Cawood, P.A.; Hawkesworth, C.J.; Dhuime, B. Detrital Zircon Record and Tectonic Setting. *Geology* **2012**, *40*, 875–878. [CrossRef]
76. Lee, C.T.A.; Bachmann, O. How Important Is the Role of Crystal Fractionation in Making Intermediate Magmas? Insights from Zr and P Systematics. *Earth Planet. Sci. Lett.* **2014**, *393*, 266–274. [CrossRef]
77. Borg, S.G.; Stump, E.; Chappell, B.W.; McCulloch, M.T.; Wyborn, D.; Armstrong, R.L.; Holloway, J.R. Granitoids of Northern Victoria Land, Antarctica; Implications of Chemical and Isotopic Variations to Regional Crustal Structure and Tectonics. *Am. J. Sci.* **1987**, *287*, 127–169. [CrossRef]
78. Rocchi, S.; Tonarini, S.; Armienti, P.; Innocenti, F.; Manetti, P. Geochemical and Isotopic Structure of the Early Palaeozoic Active Margin of Gondwana in Northern Victoria Land, Antarctica. *Tectonophysics* **1998**, *284*, 261–281. [CrossRef]
79. Paulsen, T.S.; Encarnación, J.; Grunow, A.M.; Layer, P.W.; Watkeys, M. New Age Constraints for a Short Pulse in Ross Orogen Deformation Triggered by East-West Gondwana Suturing. *Gondwana Res.* **2007**, *12*, 417–427. [CrossRef]
80. Goodge, J.W.; Dallmeyer, R.D. Contrasting Thermal Evolution within the Ross Orogen, Antarctica: Evidence from Mineral Ages. *J. Geol.* **1996**, *104*, 435–458. [CrossRef]
81. Goodge, J.W.; Dallmeyer, R.D. 40Ar/39Ar Mineral Age Constraints on the Paleozoic Tectonothermal Evolution of High-Grade Basement Rocks within the Ross Orogen, Central Transantarctic Mountains. *J. Geol.* **1992**, *100*, 91–106. [CrossRef]
82. Talarico, F.M.; Stump, E.; Gootee, B.F.; Foland, K.A.; Palmeri, R.; van Schmus, W.R.; Brand, P.K.; Ricci, C.A. First Evidence of a "Barrovian"-Type Metamorphic Regime in the Ross Orogen of the Byrd Glacier Area, Central Transantarctic Mountains. *Antarct. Sci.* **2007**, *19*, 451–470. [CrossRef]
83. Takigami, Y.; Watanabe, T. 40Ar-39Ar Geochronological Studies of Granitic Rocks from South Victoria Land, Antarctica. In Proceedings of the NIPR Symposium on Antarctic Geosciences, Tokyo, Japan, 26–27 October 1995; National Institute of Polar Research: Tokyo, Japan, 1995; Volume 8, pp. 160–168.
84. Allibone, A.; Wysoczanski, R. Initiation of Magmatism during the Cambro-Ordovician Ross Orogeny in Southern Victoria Land, Antarctica. *Geol. Soc. Am. Bull.* **2002**, *114*, 1007–1018. [CrossRef]
85. Cook, Y.A.; Craw, D. Amalgamation of Disparate Crustal Fragments in the Walcott Bay-Foster Glacier Area, South Victoria Land, Antarctica. *N. Z. J. Geol. Geophys.* **2001**, *44*, 403–416. [CrossRef]
86. Cooper, A.F.; Worley, B.A.; Armstrong, R.A.; Price, R.C. Synorogenic Alkaline and Carbonatitic Magmatism in the Transantarctic Mountains of South Victoria Land, Antarctica. In *The Antarctic Region: Geological Evolution and Processes*; Ricci, C.A., Ed.; Terra Antartica Publications: Siena, Italy, 1997; pp. 191–202.
87. Cottle, J.M.; Cooper, A.F. Geology, Geochemistry, and Geochronology of an A-type Granite in the Mulock Glacier Area, Southern Victoria Land, Antarctica. *N. Z. J. Geol. Geophys.* **2006**, *49*, 191–202. [CrossRef]
88. Cottle, J.M.; Cooper, A.F. The Fontaine Pluton: An Early Ross Orogeny Calc-Alkaline Gabbro from Southern Victoria Land, Antarctica. *N. Z. J. Geol. Geophys.* **2006**, *49*, 177–189. [CrossRef]
89. Cox, S.C.; Parkinson, D.L.; Allibone, A.H.; Cooper, A.F. Isotopic Character of Cambro-Ordovician Plutonism, Southern Victoria Land, Antarctica. *N. Z. J. Geol. Geophys.* **2000**, *43*, 501–520. [CrossRef]
90. Goodge, J.W.; Walker, N.W.; Hansen, V.L. Neoproterozoic-Cambrian Basement-Involved Orogenesis within the Antarctic Margin of Gondwana. *Geology* **1993**, *21*, 37–40. [CrossRef]

91. Hagen-Peter, G.; Cottle, J.M. Synchronous Alkaline and Subalkaline Magmatism during the Late Neoproterozoic—Early Paleozoic Ross Orogeny, Antarctica: Insights into Magmatic Sources and Processes within a Continental Arc. *Lithos* **2016**, *262*, 677–698. [CrossRef]
92. Martin, A.P.; Cooper, A.F.; Price, R.C.; Turnbull, R.E.; Roberts, N.M.W. The Petrology, Geochronology and Significance of Granite Harbour Intrusive Complex Xenoliths and Outcrop Sampled in Western McMurdo Sound, Southern Victoria Land, Antarctica. *N. Z. J. Geol. Geophys.* **2015**, *58*, 33–51. [CrossRef]
93. Mellish, S.D.; Cooper, A.F.; Walker, N.W. Panorama Pluton: A Composite Gabbro-Monzodiorite Early Ross Orogeny Intrusion in Southern Victoria Land, Antarctica. In *Antarctica at the Close of a Millennium, The Royal Society of New Zealand Bulletin 35*; Gamble, J.A., Skinner, D.N.B., Henrys, S., Eds.; Royal Society of New Zealand: Wellington, New Zealand, 2002; pp. 125–141.
94. Read, S.E. Koettlitz Glacier Alkaline Province: Late Neoproterozoic Extensional Magmatism in Southern Victoria Land, Antarctica. Ph.D. Thesis, University of Otago, Otago, New Zealand, 2010.
95. Read, S.E.; Cooper, A.F.; Walker, N.W. Geochemistry and U-Pb Geochronology of the Neoproterozoic-Cambrian Koettlitz Glacier Alkaline Province, Royal Society Range, Transantarctic Mountains, Antarctica. In *Antarctica at the Close of a Millennium, Royal Society of New Zealand Bulletin 35*; Gamble, J.A., Skinner, D.N.B., Henrys, S., Eds.; Royal Society of New Zealand: Wellington, New Zealand, 2002; pp. 143–151.
96. Rowell, A.; Rees, M.; Duebendorfer, E. An Active Neoproterozoic Margin: Evidence from the Skelton Glacier Area, Transantarctic Mountains. *J. Geol. Soc. Lond.* **1993**, *150*, 677–682. [CrossRef]
97. Stump, E.; Gootee, B.; Talarico, F. Tectonic Model for Development of the Byrd Glacier Discontinuity and Surrounding Regions of the Transantarctic Mountains during the Neoproterozoic-Early Paleozoic. In *Antarctica: Contributions to Global Earth Sciences*; Futterer, D., Damaske, D., Kleinschmidt, G., Miller, H., Tessensohn, F., Eds.; Springer: Berlin/Heidelberg, Germany; New York, NY, USA, 2006; pp. 181–190.
98. Wysoczanski, R.J.; Allibone, A.H. Age, Correlation, and Provenance of the Neoproterozoic Skelton Group, Antarctica: Grenville Age Detritus on the Margin of East Antarctica. *J. Geol.* **2004**, *112*, 401–4156. [CrossRef]
99. Goodge, J.W.; Fanning, C.M.; Norman, M.D.; Bennett, V.C. Temporal, Isotopic and Spatial Relations of Early Paleozoic Gondwana-Margin Arc Magmatism, Central Transantarctic Mountains, Antarctica. *J. Petrol.* **2012**, *53*, 2027–2065. [CrossRef]
100. Hagen-Peter, G.; Cottle, J.M.; Tulloch, A.J.; Cox, S.C. Mixing between Enriched Lithospheric Mantle and Crustal Components in a Short-Lived Subduction-Related Magma System, Dry Valleys Area, Antarctica: Insights from U-Pb Geochronology, Hf Isotopes, and Whole-Rock Geochemistry. *Lithosphere* **2015**, *7*, 174–188. [CrossRef]
101. Hagen-Peter, G.; Cottle, J.M.; Smit, M.; Cooper, A.F. Coupled Garnet Lu-Hf and Monazite U-Pb Geochronology Constrain Early Convergent Margin Dynamics in the Ross Orogen, Antarctica. *J. Metamorph. Geol.* **2016**, *34*, 293–319. [CrossRef]
102. Paulsen, T.S.; Deering, C.; Sliwinski, J.; Bachmann, O.; Guillong, M. Detrital Zircon Ages from the Ross Supergroup, North Victoria Land, Antarctica: Implications for the Tectonostratigraphic Evolution of the Pacific-Gondwana Margin. *Gondwana Res.* **2016**, *35*, 79–96. [CrossRef]
103. Yi, S.B.; Lee, M.J.; Lee, J.I.; Kim, H. Timing and Metamorphic Evolution of the Ross Orogeny in and around the Mountaineer Range, Northern Victoria Land, Antarctica. *Minerals* **2020**, *10*, 908. [CrossRef]
104. Welke, B.; Licht, K.; Hennessy, A.; Hemmin, S.; Davis, E.P.; Kassab, C. Applications of Detrital Geochronology and Thermochronology from Glacial Deposits to the Paleozoic and Mesozoic Thermal History of the Ross Embayment, Antarctica Bethany. *Geochem. Geophys. Geosyst.* **2016**, *17*, 2762–2780. [CrossRef]
105. Palmer, E.F.; Licht, K.J.; Swope, R.J.; Hemming, S.R. Nunatak Moraines as a Repository of What Lies beneath the East Antarctic Ice Sheet. *Spec. Pap. Geol. Soc. Am.* **2012**, *487*, 97–104. [CrossRef]
106. Glen, R.A.; Cooper, R.A. Evolution of the East Gondwana Convergent Margin in Antarctica, Southern Australia and New Zealand from the Neoproterozoic to Latest Devonian. *Earth Sci. Rev.* **2021**, *220*, 103687. [CrossRef]
107. Stump, E.; Smit, J.H.; Self, S. Timing of Events during the Late Proterozoic Beardmore Orogeny, Antarctica: Geological Evidence from the La Gorce Mountains. *Geol. Soc. Am. Bull.* **1986**, *97*, 953–965. [CrossRef]
108. Brown, D.A.; Hand, M.; Morrissey, L.J.; Goodge, J.W. Cambrian Eclogite-Facies Metamorphism in the Central Transantarctic Mountains, East Antarctica: Extending the Record of Early Palaeozoic High-Pressure Metamorphism along the Eastern Gondwanan Margin. *Lithos* **2020**, *366–367*, 105571. [CrossRef]
109. Talarico, F.M.; Findlay, R.H. Metamorphic Evolution of the Koettlitz Group in the Koettlitz-Ferrar Glaciers Region (Southern Victoria Land, Antarctica). *Terra Antart.* **2005**, *12*, 3–23.
110. Collins, W.J. Hot Orogens, Tectonic Switching, and Creation of Continental Crust. *Geology* **2002**, *30*, 535–538. [CrossRef]
111. Jarrard, R.D. Relations among Subduction Parameters. *Rev. Geophys.* **1986**, *24*, 217–284. [CrossRef]
112. Barth, A.P.; Wooden, J.L.; Jacobson, C.E.; Economos, R.C. Detrital Zircon as a Proxy for Tracking the Magmatic Arc System: The California Arc Example. *Geology* **2013**, *41*, 223–226. [CrossRef]
113. Ducea, M.N.; Saleeby, J.B.; Bergantz, G. The Architecture, Chemistry, and Evolution of Continental Magmatic Arcs. *Annu. Rev. Earth Planet. Sci.* **2015**, *43*, 299–331. [CrossRef]
114. Nelson, D.A.; Cottle, J.M. Long-Term Geochemical and Geodynamic Segmentation of the Paleo-Pacific Margin of Gondwana: Insight from the Antarctic and Adjacent Sectors. *Tectonics* **2017**, *36*, 3229–3247. [CrossRef]
115. Squire, R.J.; Wilson, C.J.L. Interaction between Collisional Orogenesis and Convergent-Margin Processes: Evolution of the Cambrian Proto-Pacific Margin of East Gondwana. *J. Geol. Soc.* **2005**, *162*, 749–761. [CrossRef]

116. Armstrong, R.; De Wit, M.J.; Reid, D.; York, D.; Zartman, R. Cape Town's Table Mountain Rapid Pan African Uplift of Its Basement Rocks. *J. Afr. Earth Sci.* **1998**, *27*, 10–11.
117. Duebendorfer, E.M.; Rees, M.N. Evidence for Cambrian Deformation in the Ellsworth-Whitmore Mountains Terrane, Antarctica: Stratigraphic and Tectonic Implications. *Geology* **1998**, *26*, 55–58. [CrossRef]
118. Curtis, M.L. Tectonic History of the Ellsworth Mountains, West Antarctica: Reconciling a Gondwana Enigma. *Geol. Soc. Am. Bull.* **2001**, *113*, 939–958. [CrossRef]
119. Millar, I.L.; Storey, B.C. Early Palaeozoic Rather than Neoproterozoic Volcanism and Rifting within the Transantarctic Mountains. *J. Geol. Soc. Lond.* **1995**, *152*, 417–420. [CrossRef]
120. Curtis, M.L.; Millar, I.L.; Storey, B.C.; Fanning, M. Structural and Geochronological Constraints of Early Ross Orogenic Deformation in the Pensacola Mountains, Antarctica. *Bull. Geol. Soc. Am.* **2004**, *116*, 619–636. [CrossRef]
121. Foster, D.A.; Gray, D.R.; Spaggiari, C. Timing of Subduction and Exhumation along the Cambrian East Gondwana Margin, and the Formation of Paleozoic Backarc Basins. *Geol. Soc. Am. Bull.* **2005**, *117*, 105–116. [CrossRef]
122. Rowell, A.J.; van Schmus, W.R.; Storey, B.C.; Fetter, A.H.; Evans, K.R. Latest Neoproterozoic to Mid-Cambrian Age for the Main Deformation Phases of the Transantarctic Mountains: New Stratigraphic and Isotopic Constraints from the Pensacola Mountains, Antarctica. *J. Geol. Soc. Lond.* **2001**, *158*, 295–308. [CrossRef]